Magnetic control of a two-layer pipe flow

S.H. Ferguson Briggs* and A.J. Mestel

Imperial College London, Exhibition Road,

South Kensington, London, SW7 2BX, UK

M.G. Blyth

University of East Anglia, Research Park, Norwich, NR4 7TJ, UK

(Dated: October 17, 2025)

Abstract

The gap between two solid, coaxial cylinders is filled with two ferrofluids of differing viscosity and magnetic susceptibility. Axial motion is driven by a pressure gradient and/or translation of the inner cylinder. An axial magnetic field is imposed externally, while current flowing in the inner cylinder generates an azimuthal field. It is known that the axisymmetric capillary instability of the cylindrical fluid interface may be controlled either by hydrodynamic shear or magnetic effects, but each of these can give rise to other instabilities, often non-axisymmetric. This paper investigates the ten-dimensional parameter space to determine when combined action of shear and magnetic effects can provide overall stability, essentially using shear to stabilise the troublesome helical 'tearing' mode, while magnetic stresses control the hydrodynamic instability. Stability is easier to obtain when the inner fluid is more magnetic.

I. INTRODUCTION

In recent years it has been shown that a cylindrical column of magnetisable ferrofluid, ordinarily prone to a Plateau-Rayleigh instability, can be stabilised by applying a magnetic field. Ferrofluids are stable colloidal suspensions of small magnetic particles in a carrier solution. They behave as viscous fluids and become magnetised in the presence of a magnetic field. Originally developed by NASA for vibration dampening purposes, ferrofluids have since been utilised in numerous applications ranging from audio speakers to hyperthermia treatment [1]. Of most relevance here is their use in ink jet printing [2, 3], magnetic drug targeting [4–6], enhanced fluid-transportation [7] and drag reduction [8]. The stability of the interface that arises in such systems is crucial for reliability and control. In particular, ink jet printing, slot-die coating and drug targetting are well-modelled by rod-annular flow [9, 10], motivating the exploration of a two-ferrofluid rod-annular flow (RAF). RAF involves two concentric cylindrical fluid annuli in axial motion, centred on a solid rod and enclosed by an outer cylinder.

In this work we consider a flow driven by an axial pressure gradient and/or translation of the rod in either direction. An azimuthal magnetic field, whose strength decreases as the reciprocal of the radius, is generated by a current running through the rod. An axial field of

* sf218@ic.ac.uk

constant strength is also applied, and this can be thought of as being produced by a solenoid wrapped around the outer cylinder.

Cylindrical interfaces are inherently unstable due to capillary action [11–14]. Yet, an azimuthal magnetic field can stabilise the interface. References [15], [16], and [17] proved that for a sufficiently strong current, such that the magnetic Bond number B satisfies $B > 1$, an irrotational, inviscid ferrofluid jet is stabilised. References [16] and [18] highlighted the importance of including viscous effects in the theory. This was supported by Ref. [19], who provided a theoretical analysis for axisymmetric disturbances to a Newtonian ferrofluid jet centred on a current-carrying wire. They found that while the condition $B > 1$ is still required for stability, including viscous effects in the analysis leads to better agreement with the experimental results. These authors also derived a dispersion relation in the case when an axial field is acting. Although the axial field exerts a stabilising effect, it cannot control long waves in the axial direction. In a bid to model magnetic drug targeting, Ref. [20] studied a non-magnetic viscous fluid surrounding a ferrofluid jet. Both the viscosity ratio and the density ratio appear in the dispersion relation, but $B > 1$ remains as the critical condition for stability. Reference [21] allowed the outer fluid to be a ferrofluid with lower magnetic susceptibility contained within a cuvette, and confirmed that axisymmetric disturbances are still stabilised if $B > 1$. Below the critical field strength, the relative fluid thicknesses were found to determine the size of the drops once the jet disintegrates.

Reference [22] (henceforth referred to as FBM) explored the effect of azimuthal and axial fields, applied independently or simultaneously, for a stationary two-ferrofluid system with the outer ferrofluid unbounded. The magnetic forcing is only felt by the fluid at the interface, where a discontinuity in the magnetic susceptibility exists. It therefore acts as a magnetic pressure, influencing the deformation of the cylindrical interface, alongside surface tension effects. While the azimuthal field stabilises the system when the inner fluid is more magnetic, it is destabilising when the outer fluid is more magnetic, a consequence of the azimuthal field strength decreasing radially. For a minimum-energy configuration, the fluid with the highest magnetisation should align with the strongest region of the azimuthal field. When this alignment is disrupted, such as when the outer-fluid is more magnetic, instability is generated by the magnetic forcing. In the latter case, FBM found that non-axisymmetric modes are important. In contrast the axial field has a stabilising effect irrespective of which fluid is more magnetic, although long waves in the axial direction remain unstable

in agreement with the findings of Ref. [19]. When both fields are applied simultaneously, stability can only be achieved if the inner fluid is the more magnetic, since otherwise long-wave instabilities persist as the field strength increases. Work on nonlinear disturbances to ferrofluid jets has revealed the existence of solitary waves [18, 23, 24]. In this paper we restrict our attention to small amplitude, linear disturbances.

In the absence of magnetic effects, capillary instability can be controlled by a sufficiently strong viscous shear force at the interface, although this may also lead to further hydrodynamic instabilities. If there is no rod the set-up is typically referred to as core-annular flow (CAF). Numerous works (eg. [25–29]; see Ref. [30], henceforth referred to as FBBM, for a detailed review), conclude that for a range of pressure-driven flow strengths a stable CAF system is possible if the inner fluid is the more viscous, but the system is always unstable if the outer fluid is the more viscous. With an axial rod present, Ref. [9] found that it is advantageous for the outer fluid to be the more viscous for certain rod speeds. More recently, FBBM investigated RAF with both a moving rod and a driving pressure gradient. It was shown that, for a stationary rod and a range of pressure gradients, stability can also be achieved when the outer fluid is more viscous provided that the rod radius is large enough.

Reference [31] found that non-axisymmetric modes can be important when the pressure gradient is sufficiently strong. FBBM argued that unstable non-axisymmetric modes result from the background shear, similar to what was observed by Ref. [32] for annular Poiseuille flow. These modes are largely unaffected by capillary forcing and only occur for specific fluid thickness ratios. Changing the parameter values, or moving the rod in the opposite direction to the base flow, can remove these modes. FBBM also found that non-axisymmetric modes can be the most unstable at moderate base flow strengths when the outer fluid is more viscous and the rod is stationary, and for all base flow strengths when the rod is moving irrespective of which fluid is the more viscous. When the rod is stationary, there always exist configurations with unstable pressure-driven flow strengths, and translating the rod can have either a stabilising or destabilising influence depending on the parameter values. Moreover, for certain pipe and rod radii, the system may be unstable irrespective of the strength of the pressure-driven flow or rod speed.

In the absence of a magnetic field the configuration studied here reduces to that examined by FBBM. Our goal is to investigate the influence of magnetic effects on the stability picture for the RAF configuration in FBBM, with particular emphasis on the coupling between

magnetic and base-flow effects. Previous studies [[33], [8]] have demonstrated the role of magnetic fields in stabilising flow instabilities. Reference [33] analysed the effect of a constant axial magnetic field on a magnetic jet sheared by a surrounding non-magnetic fluid, showing that the field can stabilise the flow in the inviscid limit. More recently, Ref. [8] showed experimentally that drag can be reduced in a viscous channel flow by including a ferrofluid film held in place at the upper-wall of the channel by a magnetic field. They observed interfacial instabilities at high flow rates that are dampened by amplifying the field strength. Preliminary work by the authors [34] examined the stability of the FBBM system with ferrofluids of varying susceptibility, with the inner fluid more viscous, and flow generated by a pressure gradient in the axial direction. In contrast to Ref. [33], the viscous two-fluid system is bounded by an outer wall and a current-carrying rod runs along the jet axis. For the parameters considered, Ref. [34] find an azimuthal field, generated by the current in the rod, stabilises unstable flow strengths when the inner fluid is more magnetic, but otherwise induces unstable modes. An axial field can produce a larger range of stable base-flows independently, provided long-waves are hydrodynamically stable, and when applied in conjunction with the azimuthal field, helical modes are produced with both stabilising and destabilising effects. In particular, Ref. [34] highlights the complexity of the coupling of the field and flow, and motivates this study. Here, we extend the analysis undertaken by Ref. [34] to cases where the outer fluid is more viscous and the rod is in motion, thereby generating different base flow profiles. We also investigate newly observed magnetic instabilities.

The structure of the paper is as follows. In Section II we formulate the problem. In Section III numerical results are given, when the rod is stationary (Section III A) and when the rod moves axially (Section III B). In particular, we focus on the unstable regions 1, 2 and 3 identified in FBBM, and also study configurations that are unstable for all flow strengths when there is no field. The effect of the azimuthal and axial fields are investigated, both independently and together, when either fluid is more magnetic. In general, the azimuthal field is found to be stabilising when the inner fluid is more magnetic, and the axial field will have a stabilising effect irrespective of the sign of the magnetic susceptibility jump at the interface. Regions 1, 2, and 3 can be shifted by different field orientations and strengths, and with different rod speeds. Interestingly, too large field strengths can lead to new magnetic instabilities, and these are investigated both for stationary and moving rods. We conclude in Section IV.

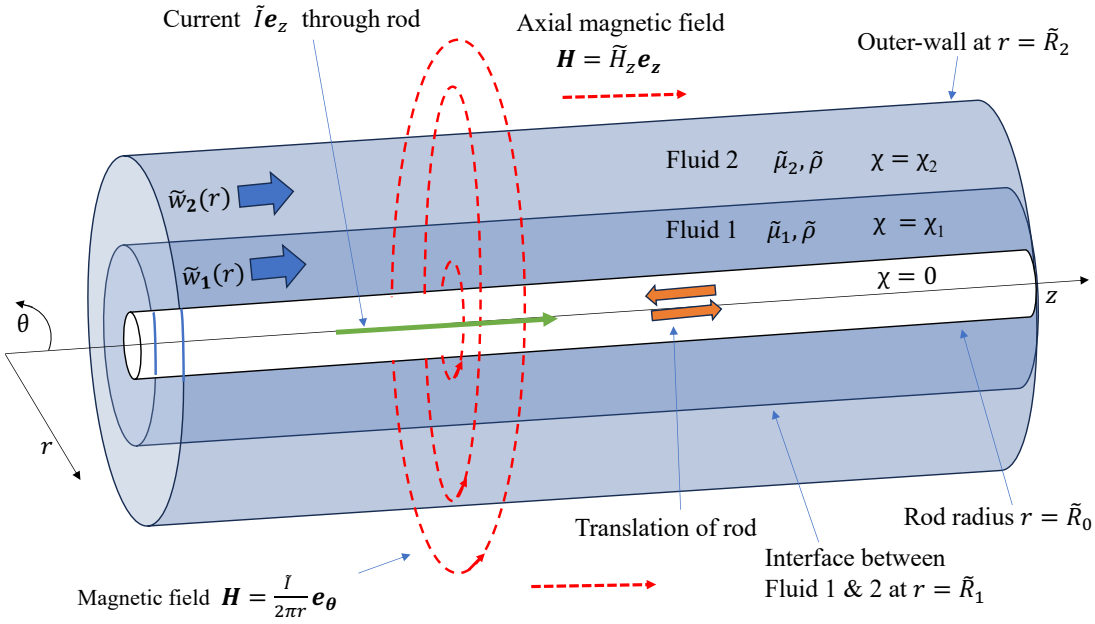

FIG. 1: Schematic of the base-state.

II. FORMULATION

We consider the flow through a circular cylindrical pipe of two incompressible, immiscible ferrofluids of different viscosities and magnetic susceptibilities. A cylindrical rod along the pipe axis carries an electric current of strength $\widetilde{I}$ that generates an azimuthal magnetic field. An axial magnetic field of strength $\widetilde{H}_z$ is also applied to the system. To describe the problem set-up we use cylindrical polar co-ordinates (r, θ, z), where z points along the rod, and $\boldsymbol{e}_r$, $\boldsymbol{e}_\theta$, $\boldsymbol{e}_z$ are the corresponding unit vectors (see Figure 1). The rod has radius $\widetilde{R}_0$ and the pipe wall has radius $\widetilde{R}_2$. The two fluids are arranged in concentric annuli, with the interface at $r = \widetilde{R}_1$ in the undisturbed base state, so that fluid 1 occupies $\widetilde{R}_0 < r < \widetilde{R}_1$ and fluid 2 fills $\widetilde{R}_1 < r < \widetilde{R}_2$, as shown in Figure 1. The fluids are assumed to have the same density, $\widetilde{\rho}$, so that gravity does not affect the system. Flow through the pipe is driven by an axial pressure gradient of strength $\widetilde{G}$, which acts in the positive z direction, and by the axial translation of the rod at speed $\widetilde{W}$ in either direction. We also consider the case when the rod is stationary. The undisturbed basic flow has velocity $\widetilde{w}(r)\boldsymbol{e}_z$.

In both fluids, the magnetisation is assumed to be collinear with the local field, $\boldsymbol{H}$, such that the induced field $\boldsymbol{B}$ satisfies

$$\boldsymbol{B} = \mu_0(1 + \chi)\boldsymbol{H}, \tag{1}$$

where μ_0 is the vacuum permeability and χ is the magnetic susceptibility of each fluid with $\chi = \chi_1$ in fluid 1 and $\chi = \chi_2$ in fluid 2. Gauss's law therefore gives

$$\boldsymbol{\nabla} \cdot \big((1+\chi)\boldsymbol{H}\big) = 0. \tag{2}$$

Continuity conditions on the magnetic field are applied at $r = \tilde{R}_0$, $\tilde{R}_2$ and $\tilde{R}(\theta, z, t)$, where the latter is the location of the disturbed fluid-fluid interface. For the normal component of $\boldsymbol{B}$ we impose

$$[\mu_0(1+\chi)\boldsymbol{H} \cdot \boldsymbol{n}] = 0, \tag{3}$$

and for the tangential components of $\boldsymbol{H}$ we impose,

$$[\boldsymbol{H} \cdot \boldsymbol{\tau}] = 0, \tag{4}$$

where $\boldsymbol{n}$ and $\boldsymbol{\tau}$ are respectively the unit normal and tangential vectors to the interface or wall/rod, and the square brackets denote the jump across the boundary. Here $\boldsymbol{\tau}$ denotes either of the tangent vectors. Within each ferrofluid the susceptibility χ is constant, so that the stress tensor is given by

$$\mathbf{T} = \mu_0(1+\chi)\left(\boldsymbol{H}\boldsymbol{H}^{\boldsymbol{T}} - \frac{1}{2}H^2\mathbf{I}\right) - p\mathbf{I} + \widetilde{\mu}(\nabla\boldsymbol{u} + (\nabla\boldsymbol{u})^T), \tag{5}$$

where $H = |\boldsymbol{H}|$, while $\widetilde{\mu}$, $\boldsymbol{u}$ and p are the dynamic viscosity, velocity and pressure in each fluid [35]. Furthermore, in fluids 1 and 2, which are assumed to be current-free,

$$\boldsymbol{\nabla} \times \boldsymbol{H} = 0. \tag{6}$$

Since the magnetic terms in Equation (5) are divergence-free, the flow in each fluid is governed by the unforced incompressible Navier-Stokes equations

$$\boldsymbol{\nabla} \cdot \boldsymbol{u} = 0, \qquad \widetilde{\rho}\,\frac{D\boldsymbol{u}}{Dt} + \boldsymbol{\nabla} p = \widetilde{\mu}\,\boldsymbol{\nabla}^2\boldsymbol{u}. \tag{7}$$

The magnetic effects are coupled to the velocity fields through the continuity of stress condition at the fluid-fluid interface at $r = \tilde{R}$. Specifically,

$$\widetilde{\sigma}\boldsymbol{\nabla} \cdot \boldsymbol{n} = [\boldsymbol{n} \cdot \mathbf{T} \cdot \boldsymbol{n}]_1^2, \qquad [\boldsymbol{n} \cdot \mathbf{T} \cdot \boldsymbol{\tau}]_1^2 = 0, \tag{8}$$

where $\widetilde{\sigma}$ is the coefficient of surface tension and $\boldsymbol{n} = (1, 0, 0)^T$ in the base-state. The kinematic condition at the disturbed interface requires

$$\frac{D}{Dt}\big(\widetilde{R}(\theta, z, t) - r\big) = 0 \tag{9}$$

at $r = \widetilde{R}$. We also require continuity of velocity at the interface, and we apply no-slip boundary conditions at the rod and the wall. The latter requires the axial flow in the base-state to be equal to $\widetilde{W}$ at $r = \widetilde{R}_0$.

The total applied field comprising of both azimuthal and axial components is denoted by $\widetilde{\boldsymbol{H}}$ and given as

$$\widetilde{\boldsymbol{H}} = \frac{\widetilde{I}r}{2\pi\widetilde{R}_0^2}\boldsymbol{e}_\theta + \widetilde{H}_z\boldsymbol{e}_z, \quad 0 \le r \le \widetilde{R}_0 \tag{10}$$

and

$$\widetilde{\boldsymbol{H}} = \frac{\widetilde{I}}{2\pi r}\boldsymbol{e}_{\boldsymbol{\theta}} + \widetilde{H}_z\boldsymbol{e}_z, \quad r > \widetilde{R}_0, \tag{11}$$

where $\widetilde{I}$ is the current in the wire.

We non-dimensionalise the problem using the length scale $\widetilde{R}_1$, the velocity scale $\widetilde{\sigma}/\widetilde{\mu}_1$, the pressure scale $\widetilde{\sigma}/\widetilde{R}_1$ and the time-scale $\widetilde{R}_1\widetilde{\mu}_1/\widetilde{\sigma}$, where $\widetilde{\mu}_\iota$ are the fluid dynamic viscosities. We non-dimensionalise the magnetic field using the scale $\widetilde{I}/(2\pi\widetilde{R}_1)$. From here on the variables are dimensionless, and we denote the dimensionless pressure and velocity by p and $\mathbf{u} = (u, v, w)^T$, where u, v, w are respectively the radial, azimuthal and axial components. The following ten parameters appear in the non-dimensionalised governing equations. Firstly R_0 and R_2 denote the dimensionless rod radius and the outer-wall radius,

$$R_0 = \frac{\widetilde{R}_0}{\widetilde{R}_1}, \qquad R_2 = \frac{\widetilde{R}_2}{\widetilde{R}_1}, \tag{12}$$

while χ_1 and χ_2 are the magnetic susceptibilities of the two fluids. Then

$$\mu = \frac{\widetilde{\mu}_2}{\widetilde{\mu}_1} \tag{13}$$

is the viscosity ratio of the fluids,

$$G = \frac{\widetilde{\rho}\widetilde{G}\widetilde{R}_1^3}{\widetilde{\mu}_1^2} \ge 0 \tag{14}$$

measures the strength of the driving pressure-gradient,

$$W = \frac{\widetilde{\rho}\widetilde{W}\widetilde{R}_1}{\widetilde{\mu}_1} \lesseqgtr 0, \tag{15}$$

is the magnitude of the axial velocity of the rod (which can take either sign),

$$J = \frac{\widetilde{\rho}\widetilde{R}_1\widetilde{\sigma}}{\widetilde{\mu}_1^2} \tag{16}$$

is a measure of the strength of capillary forcing,

$$B = \frac{\mu_0 \widetilde{I}^2}{4\pi^2 \widetilde{\sigma} \widetilde{R}_1} \tag{17}$$

compares the square of the azimuthal magnetic field to surface tension and

$$Z = \frac{\widetilde{H}_z}{\widetilde{I}/2\pi\widetilde{R}_1} \tag{18}$$

is the ratio of the effective strength of the axial field to azimuthal field. The relative strength of axial field to surface tension is measured by BZ^2. Our choice of the capillary velocity scale makes it easier to focus on the interface behaviour where the magnetic field interacts with the fluid, and permits direct comparison with FBBM and FBM. For convenience we also use a switch parameter I where $I = 1$ if a current flows in the rod, and $I = 0$ if it does not. We note that when no current flows $B = 0$ and Z is formally infinite, but BZ^2 remains finite and is an appropriate measure of the magnetic field strength.

The dimensionless field in the basic state is given by

$$\overline{\boldsymbol{H}} = \frac{Ir}{R_0^2}\boldsymbol{e}_\theta + Z\boldsymbol{e}_z, \quad 0 \le r \le R_0 \tag{19}$$

in the rod, and

$$\overline{\boldsymbol{H}} = \frac{I}{r}\boldsymbol{e}_{\boldsymbol{\theta}} + Z\boldsymbol{e}_z, \quad R_0 < r \tag{20}$$

outside the rod. The dimensionless base flow is unchanged from FBBM, but is given here for reference. The flow is solely in the axial direction and is given in fluids 1 and 2 respectively as

$$\overline{w}_1 = \frac{G}{4J}(R_0^2 - r^2 + a\ln\frac{r}{R_0}) + \frac{W}{J}(1 - b\ln\frac{r}{R_0}) \tag{21}$$

$$\overline{w}_2 = \frac{G}{4\mu J}(R_2^2 - r^2 + a\ln\frac{r}{R_2}) - \frac{Wb}{\mu J}\ln\frac{r}{R_2} \tag{22}$$

where

$$a = \frac{R_2^2 - 1 + \mu(1 - R_0^2)}{\ln R_2 - \mu \ln R_0}, \qquad b = \frac{\mu}{\ln R_2 - \mu \ln R_0}. \tag{23}$$

The pressure in the base state is determined using the axial momentum equation and the normal stress condition at the interface, giving

$$\overline{p}_1 = -\frac{Gz}{J} + p_c + 1, \qquad \overline{p}_2 = -\frac{Gz}{J} + p_c + \tfrac{1}{2}B(\chi_1 - \chi_2)\big(I + Z^2\big), \tag{24}$$

where p_c is a reference pressure that can be taken to be zero, and the third term in $\overline{p}_1$ is the effect of surface tension at the interface. The magnetic effects add an extra term to

the expression for pressure. Often, this is interpreted as a 'magnetic pressure' that acts at the interface of the fluids, and will counteract capillary action if $\chi_1 > \chi_2$, but enhance it otherwise.

A. Linearising about the base-state

In the base state the interface is located at $r = 1$. We assume a small disturbance so that the interface is displaced to the new location

$$r = 1 + \varepsilon\,\mathbb{R}(S\zeta), \qquad \text{where} \quad \zeta = \exp(\mathrm{i}(kz + m\theta) + st), \tag{25}$$

$\varepsilon \ll 1$, $k \in \mathbb{R}$ and $m \in \mathbb{Z}$ are given wave-numbers, and $s \equiv s_r + \mathrm{i}s_i$ is the complex growth rate. S is a constant which, if non-zero, can be normalised to unity, but is retained in the problem to allow for eigenfunctions with $S = 0$. Without loss of generality we take $k \geq 0$, and the stability results for m and $-m$ are identical unless both $I \neq 0$ and $Z \neq 0$. The real part of the perturbation is taken in (25), and this is assumed implicitly hereon for the perturbations of all variables. The velocity and pressure are assumed to take the form

$$p_\iota = \overline{p}_\iota(z) + \varepsilon\zeta\widehat{p}_\iota(r), \quad u_\iota = \varepsilon\zeta\,\widehat{u}_\iota(r), \quad v_\iota = \varepsilon\zeta\,\widehat{v}_\iota(r), \quad w_\iota = \overline{w}_\iota(r) + \varepsilon\zeta\widehat{w}_\iota(r), \tag{26}$$

and the field is perturbed as

$$\boldsymbol{H}_\iota = \overline{\boldsymbol{H}}_\iota + \varepsilon\zeta\widehat{\boldsymbol{H}}_\iota(r), \tag{27}$$

where $\iota = 0,\ 1,\ 2,\ 3$ corresponding to the rod, fluids 1, 2, and the outer wall. The current is held fixed, and therefore

$$\boldsymbol{\nabla} \times (\zeta\widehat{\boldsymbol{H}}_\iota) = \boldsymbol{0} \tag{28}$$

from Ampere's law. We define a magnetic potential $\widehat{\phi}_\iota$ such that

$$\zeta\widehat{\boldsymbol{H}}_\iota(r) = \boldsymbol{\nabla}(\zeta\widehat{\phi}_\iota(r)). \tag{29}$$

From here on we drop the hats.

Substituting (26) into the dimensionless Navier-Stokes equations, and linearising we obtain

$$(ru_\iota)' + \mathrm{i}mv_\iota + \mathrm{i}krw_\iota = 0, \tag{30}$$

$$J(s + \mathrm{i}k\overline{w}_\iota)r^2u_\iota + r^2p_\iota' = \mu^{(\iota)}\big(-2\mathrm{i}mv_\iota - u_\iota + r^2u_\iota'' + ru_\iota' - \big(m^2 + k^2r^2\big)u_\iota\big), \tag{31}$$

$$J(s+\mathrm{i}k\overline{w}_\iota)r^2v_\iota+\mathrm{i}mrp_\iota=\mu^{(\iota)}\big(-v_\iota+2\mathrm{i}mu_\iota+r^2v_\iota''+rv_\iota'-\big(m^2+k^2r^2\big)v_\iota\big),\tag{32}$$

$$J\big(u_\iota\overline{w}_\iota'+(s+\mathrm{i}k\overline{w}_\iota)\,w_\iota\big)r^2+\mathrm{i}kr^2p_\iota=\mu^{(\iota)}\big(r^2w_\iota''+rw_\iota'-\big(m^2+k^2r^2\big)w_\iota\big),\tag{33}$$

where

$$\mu^{(1)}=1,\quad \mu^{(2)}=\mu,\tag{34}$$

and $'$ corresponds to the derivative with respect to r.

Since χ is constant within fluids 1 and 2 (and zero in the rod and wall), from Gauss' Law

$$\boldsymbol{\nabla}^2(\zeta\phi_\iota)=0,\tag{35}$$

except on the fluid interface. It follows that

$$\phi''+\frac{1}{r}\phi'+\left(k^2+\frac{m^2}{r^2}\right)\phi=0,\tag{36}$$

with solution

$$\phi_\iota(r)=Q_\iota I_m(kr)+P_\iota K_m(kr),\tag{37}$$

where I_m and K_m are the modified Bessel functions of the first and second kind of order m, respectively, and Q_ι, P_ι are arbitrary constants. To avoid a singularity at $r=0$, we set $P_0=0$. The condition $\phi_{(3)}\to 0$ as $r\to\infty$ demands that $Q_3=0$. Equations (3) and (4) at $r=R_0$ and $r=R_2$ give

$$(1+\chi_1)\phi_1'=\phi_0',\quad \phi_1=\phi_0,\tag{38}$$

and

$$(1+\chi_2)\phi_2'=\phi_3',\quad \phi_2=\phi_3,\tag{39}$$

respectively. Applying (3) and (4) at the interface results in

$$(1+\chi_1)\Big(\phi_1'-\big(\mathrm{i}kZ+\mathrm{i}mI\big)S\Big)=(1+\chi_2)\Big(\phi_2'-\big(\mathrm{i}kZ+\mathrm{i}mI\big)S\Big),\quad \phi_1=\phi_2.\tag{40}$$

Equations (38)-(40) fix the remaining constants $Q_{0,1,2}$ and $P_{1,2,3}$, and their explicit forms are omitted here due to their considerable length.

The perturbed normal stress condition at the interface is

$$p_1-p_2+2\big(\mu u_2'-u_1'\big)+\Big(1-m^2-k^2-B(\chi_1-\chi_2)I\Big)S-B(\chi_2-\chi_1)\Big(imI+ikZ\Big)\phi_1=0,\tag{41}$$

and substituting the explicit solution for ϕ_1 at the interface gives

$$p_1-p_2+2\big(\mu u_2'-u_1'\big)+\Big[1-m^2-k^2-B(\chi_1-\chi_2)I-B(\chi_2-\chi_1)^2\big(mI+kZ\big)^2f\Big]S=0,\tag{42}$$

where $f > 0$ and $f \equiv f(R_0, R_2, k, m, \chi_2, \chi_1)$, omitted for brevity. Since perturbations to the magnetic potential arise in all the regions (the rod, fluid 1, fluid 2 and the outer-wall), χ_1 and χ_2 appear in f not only through contributions such as $(\chi_1 - \chi_2)$ or χ_1/χ_2, but also independently. This follows from the continuity conditions (3) and (4) at the rod and outer-wall. Interestingly, although the magnetic field is prevalent globally in the system, it only interacts with the fluid velocity locally at the interface, via Equation (42). This is a direct result of the ferrofluids being electrically insulating with piecewise constant χ. Consequently, the remaining interface conditions and boundary conditions at $r = 1$, R_0, R_2 are unchanged from FBBM, but are given here for completeness. At $r = 1$, continuity of the axial and azimuthal tangential stresses give respectively,

$$\mathrm{i}ku_1 + w_1' = \mu\big(\mathrm{i}ku_2 + w_2'\big), \quad \mathrm{i}mu_1 - v_1 + v_1' = \mu\big(\mathrm{i}mu_2 - v_2 + v_2'\big). \tag{43}$$

We note there is no magnetic contribution to the tangential stress. Continuity of $\mathbf{u}$ at the interface requires

$$u_1 = u_2, \quad v_1 = v_2, \quad w_1 + \overline{w}_1' S = w_2 + \overline{w}_2' S. \tag{44}$$

We therefore observe that the axial velocity perturbation w_ι exhibits a discontinuity due to the radial dependence of the base flow. The kinematic condition

$$sS - u_\iota + \mathrm{i}k\overline{w}_\iota S = 0, \tag{45}$$

is applied at $r = 1$. No slip at the outer-wall and rod give

$$u_2(R_2) = 0, \quad v_2(R_2) = 0, \quad w_2(R_2) = 0, \tag{46}$$

and

$$u_1(R_0) = 0, \quad v_1(R_0) = 0, \quad w_1(R_0) = 0, \tag{47}$$

respectively.

Equations (30)-(47) form an eigenvalue problem for s. A (k, m) mode is unstable if $Re(s) > 0$, and if for all modes $s_r \leq 0$, then the system is (neutrally) stable. An analytical solution exists in the Stokes limit, but we find the base flow then has no effect on the linear stability, which is therefore determined by the same stability criterion as in FBM, with the growth rate modified to include the presence of an outer wall.

For no base flow and $R_2 \to \infty$, the system studied here reduces to that examined by FBM, and many of the conclusions carry over. In this limit the stability is determined by the normal stress condition (42), and the growth rate can be written

$$s_r = \left(T_1 + T_2\right) f_1, \tag{48}$$

where

$$T_1 = 1 - m^2 - k^2 + B(\chi_2 - \chi_1)I, \quad T_2 = -B(\chi_2 - \chi_1)^2 (mI + kZ)^2 f_2, \tag{49}$$

and $f_1, f_2 > 0$. Notice that $T_2 \leq 0$, and it therefore always has a stabilising influence, or no effect when $mI + kZ = 0$, but T_1 can take either sign. If $B = 0$, $T_1 > 0$ for $m = 0$, $k < 1$ and the system is unstable to the classic Rayleigh instability. When $\chi_1 > \chi_2$ and B is sufficiently large, $T_1 < 0$ and the system can be stable. Yet if $\chi_2 > \chi_1$, increasing B will render modes of all m, k unstable. On the other hand, provided $mI + kZ \neq 0$, T_2 always has a stabilising effect, and increasing Z sufficiently stabilises all modes. If $T_1 > 0$, then for $mI + kZ = 0$, the flow will remain unstable irrespective of Z. Therefore, $k = 0$ modes remain unstable, irrespective of the strength of Z when $\chi_2 > \chi_1$. In practice, there may be some limitations on the possible axial wavelengths.

In RAF, with no magnetic field, a strong enough base flow can stabilise $0 \leq k \leq 1$ modes ([31], FBBM), but short waves are unstable if the flow is too strong. Thus, it is conceivable that appropriately chosen G, W, B, Z could result in a stable system when $\chi_2 > \chi_1$, where B and Z are such that modes with $mI + kZ = 0$ have $T_1 \geq 0$.

However, when a base-flow is present the stability is not simply governed by the normal stress, and we see other effects come into play. For arbitrary Reynolds number we must solve equations (30)-(47) numerically, and we follow the pseudo-spectral method exactly as outlined in FBBM. A truncated series of Chebyshev polynomials is employed to represent the flow variables, with the fluid domain mapped onto the canonical interval $-1 \leq x \leq 1$. Within this domain, N_1 and N_2 shifted Gauss-Lobatto collocation points are used in the interior of fluid regions 1 and 2, respectively. The momentum and continuity equations are enforced at these interior collocation points, while boundary conditions are imposed at $x = \pm 1$. Exactly as in FBBM, the spectral expansion leads to an eigenvalue problem of the form $\mathrm{A}\boldsymbol{v} = s\mathrm{B}\boldsymbol{v}$, where A, B are known matrices of size $(3(N_1 + N_2) + 7) \times (3(N_1 + N_2) + 7)$ and $\boldsymbol{v}$ is vector containing the $3(N_1 + N_2 + 2)$ unknown Chebyshev coefficients and the surface deformations S. Since the magnetic potential ϕ has an analytic solution, the modification from the

formulation in FBBM appears in a single row of A and B, corresponding to the normal stress condition. This modification affects only the columns associated with the coefficient of S. Following the same approach as in FBBM for determining convergent eigenvalues, it is found that comparable values of $N_{1,2}$ are required ($90 \leq N_{1,2} \leq 140$), and large values of the parameters B or Z require correspondingly larger values of $N_{1,2}$ for convergence. The analytical solution in the Stokes limit provides a useful check to the numerical solution. In addition, we obtain perfect agreement with FBBM when we switch off the magnetic field and with FBM when there is no base-flow and $R_2 \to \infty$.

B. Long wave limit

In the limit $k \to 0$ we find an exchange of stability only when $m = 0$. Focusing on this case, and positing the expansions

$$(u_\iota,\, v_\iota,\, kw_\iota)^T = k\mathbf{u}_{\iota 1} + k^2\mathbf{u}_{\iota 2} + \ldots \quad p_\iota = k^{-1}p_{\iota 0} + p_{\iota 1}\ldots \quad s = ks_1 + k^2 s_2 \ldots, \tag{50}$$

we find that s_1 is imaginary, and at leading order

$$s_r = k^2\left[\alpha(1 + (\chi_2 - \chi_1)IB) - \frac{1}{J}(\beta G^2 + \gamma W^2 + \delta WG)\right], \tag{51}$$

where α, β, γ, δ are known in terms of R_0, R_2 and μ. On setting $B = 0$ in (51) we recover the expression given in FBBM. The constants $\alpha > 0$ and $\beta > 0$ are given in equation (15) of [31]. The forms of γ and δ are suppressed in the interest of brevity. When $m = 0$, to leading order $\phi_1 = O(k \ln k)$ and consequently the effect of the magnetic field disturbance appears at higher order. As a result, the leading-order growth rate in (51) is independent of Z. This is confirmed by the numerical results to be shown in Figure 14 for which $G, W, B \neq 0$. Notably the intersection of the $m = 0$ neutral curve with the G axis is unchanged when Z is increased from its value in panel (b) to that in panel (c). Comparing the numerical solution for the neutral curves at $k = 0.01$ in panel (b) with the predictions of formula (51) (in brackets) for $s_r = 0$, we find $G = 551.15$ (551.53) and $G = 1825.45$ (1825.42).

For $m = 1$ we find that $\boldsymbol{u}_\iota$, p_ι and ϕ_1 are all $O(1)$ as $k \to 0$, with the effect of the base flow felt at higher order. Consequently, the leading-order approximation for s when $m = 1$ can be deduced from FBM on accounting for the presence of the pipe wall.

III. RESULTS

The system involves ten parameters, μ, R_0, R_2, χ_1, χ_2, G, W, J, B, Z, each of which influences the linear stability. It is difficult to scan the entire parameter space. We consider cases with either the inner or outer fluid being the more viscous, and one or the other to be more magnetically susceptible. The rod may be stationary or moving, while azimuthal or axial fields act either independently or simultaneously. In Section III A we consider a stationary rod, and in Section III B the rod translates in the axial direction. For ease of comparison, we present results that focus on the parameter sets studied in FBBM.

A. Stationary rod: $W = 0$

When there is no magnetic field acting, a band of stable base flow strengths $G_L \leq G \leq G_R$, can exist for certain parameters [31]. FBBM found that in general there are three regions of instability, which they labelled regions 1, 2, and 3, and these can exist for either $\mu > 1$ or $\mu < 1$. Only $m = 0$ modes are unstable in region 1, which appears as a result of capillary forcing over some range $0 \leq G \leq G_L$ ([28], [31], FBBM). Increasing the flow strength (i.e. increasing G), can dampen the capillary instability, so that instabilities from surface tension are gone for $G > G_L$. Too strong a flow, $G > G_R$, results in shear instabilities, either as region 2 or region 3 modes. Region 2 consists of interfacial shear modes with both $m = 0$ and $m \neq 0$ modes unstable. They occur because of the interfacial shear in the base flow that results from the viscosity jump. Increasing J (i.e. capillary forcing) can dampen interfacial shear modes, thereby increasing G_R, but G_L will also increase as J increases. Region 3, on the other hand, occurs as a result of the background shear, generated by the inner and outer boundaries. These shear modes were only found for particular ranges of R_0, R_2, and μ, and required significantly large G. Their stability was largely unaffected by modifying J, as the unstable modes were concentrated in critical layers near the boundaries. For large enough J, as G increases, region 3 modes become unstable before region 2, in which case G_R is given by the onset of region 3. Figure 2 shows the case when $\mu = 0.5$, $R_0 = 0.1$ and $R_2 = 1.3$ and all three regions exist. The numbers on the contours denote the real part of the growth rate s. Panels (a) and (b) show a stable band of G between regions 1 and 2 when $J = 1$. At $J = 100$ region 2 has disappeared, as can be seen in panel (c). Now, a larger range of stable G exists,

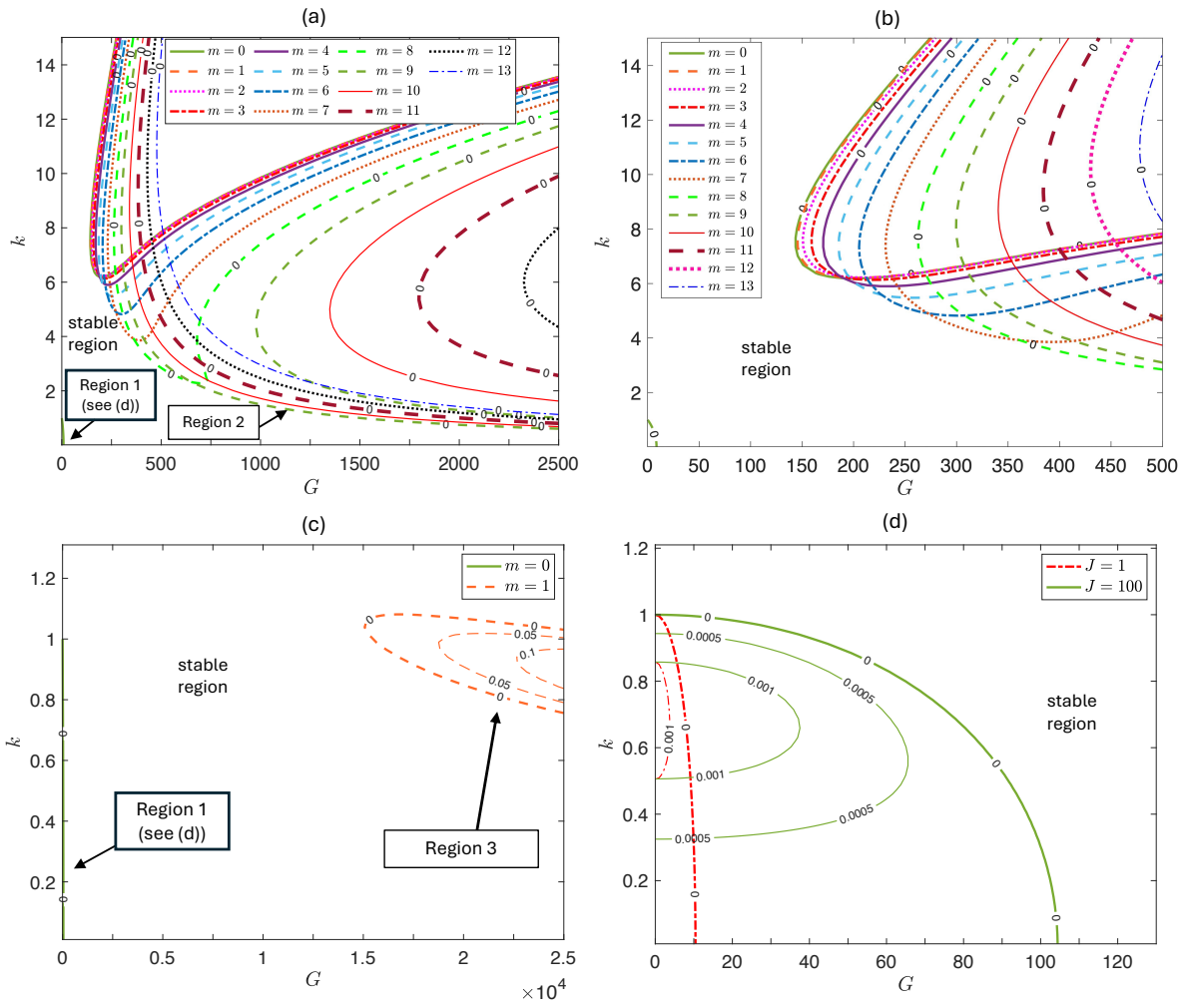

FIG. 2: Growth rates when $\mu = 0.5$, $R_2 = 1.3$, $R_0 = 0.1$, $W = 0$, $B = 0$. (a) Neutral curves when $J = 1$. Two regions of instability exist; region 1 consists of $m = 0$ unstable capillary modes for $G \leq G_L$ and region 2 consists of $m \geq 0$ interfacial modes for $G \geq G_R$. (b) Close-up of panel (a). (c) $J = 100$ and two regions of instability exist, regions 1 and 3. Increasing J has shifted region 2 to the right, so that region 2 exists past region 3, and G_R is at the onset of region 3. (d) Region 1 $m = 0$ unstable modes when $J = 1$ and $J = 100$, where G_L increases as J increases and only $m = 0$ modes are unstable. (Figure adapted from Figure 3 in FBBM)

bounded by regions 1 and 3. Panel (d) shows a superposition of region 1 when $m = 0$ for $J = 1$ (panel (a)) and $J = 100$ (panel (c)), showing that G_L increases as J is increased. The stable band between regions 1 and 2 results from a balance between capillary and frictional forces at the interface. In region 2, modes with $m > 13$ are unstable, but these lie within the

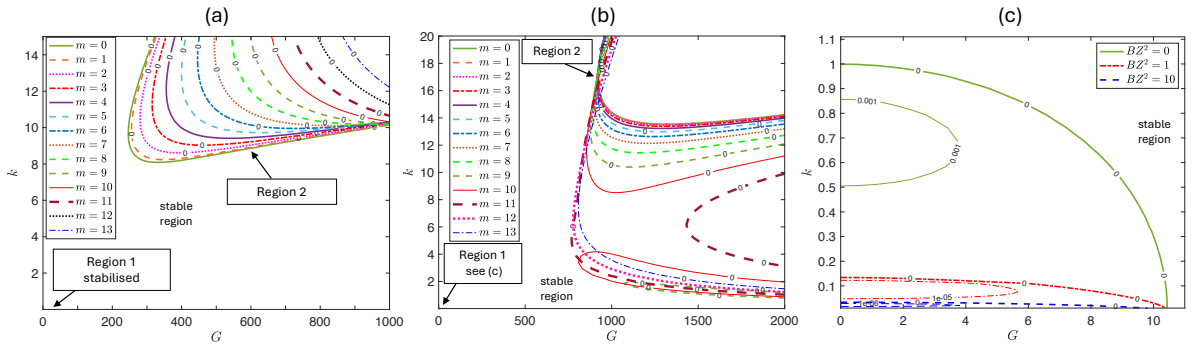

FIG. 3: Growth rates when the inner fluid is more magnetic and $\mu = 0.5$, $R_2 = 1.3$, $R_0 = 0.1$, $J = 1$, $W = 0$, $\chi_1 = 5$, $\chi_2 = 0$. (a) $B = 10$, $I = 1$, $Z = 0$ (azimuthal field on). (b) $BZ^2 = 10$, $I = 0$ (axial field on). (c) Region 1 enlarged for $m = 0$ modes and various BZ^2 values, when $I = 0$. The axial field does not stabilise region 1, since $k \to 0$ modes remain unstable. The azimuthal field can stabilise all modes in region 1. Region 2 is shifted to the right in the presence of either an azimuthal or an axial field.

unstable domain of $m = 13$ (at least up to $m = 20$). In such cases, for clarity we often omit the neutral curves for larger m. Thus in this and subsequent figures we include all neutral curves that affect the stability boundary.

We now examine the change in regions 1, 2 and 3 when an azimuthal and/or axial field is applied, when either the inner or the outer fluid is the more magnetic. When the inner fluid is more magnetic ($\chi_1 > \chi_2$), both the azimuthal and the axial fields dampen unstable modes in regions 1 and 2. Region 1 is completely stabilised for a strong enough azimuthal field (i.e. for sufficiently large B). For a strong axial field (i.e. for large BZ^2) region 1 is flattened down towards the $k = 0$ axis, but even as $BZ^2 \to \infty$, sufficiently small $k \ll 1$ remains unstable. In both cases region 2 is shifted to the right to larger G as B increases. This is shown in Figure 3 when only the inner fluid is magnetic, using the same parameters as in Figure 2. In panel (a) an azimuthal field is applied and in panel (b) an axial field is applied. Panel (c) shows that increasing the strength of the axial field squashes region 1 down towards the G-axis, stabilising all but the longest waves. In contrast, when the outer fluid is more magnetic ($\chi_2 > \chi_1$), only an axial field has a stabilising effect on regions 1 and 2, and an azimuthal field even destabilises modes with $m \neq 0$. Figure 4(a) and 4(b) show that regions 1 and 2 merge once the azimuthal field strength has reached a critical B. Comparing panel (a) for which $R_2 = 1.3$ (c.f. $B = 0$ in Figure 2) and panel (b) for which

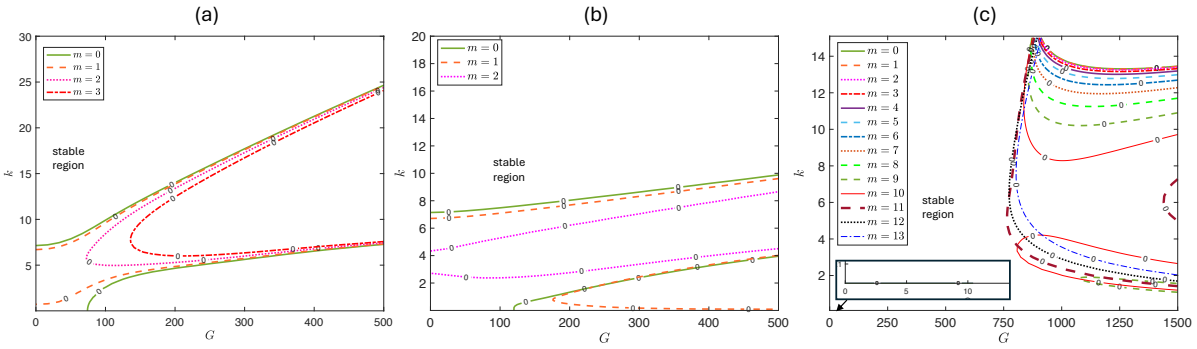

FIG. 4: Neutral curves when the outer fluid is more magnetic and $\mu = 0.5$, $R_0 = 0.1$, $J = 1$, $W = 0$, $B = 10$, $\chi_1 = 0$, $\chi_2 = 5$. In (a) $R_2 = 1.3$, $I = 1$, $Z = 0$, (b) $R_2 = 2$, $I = 1$, $Z = 0$, (c) $R_2 = 1.3$, $I = 0$, $Z = 1$. When the outer fluid is more magnetic, an axial field shifts region 2 to the right, and an azimuthal field destabilises modes so that regions 1 and 2 merge.

$R_2 = 2.0$, we observe that increasing R_2 causes $m = 1$, $k \to 0$ to become unstable, even for $G > 0$. This agrees with the results of FBM, where $m = 1$, $k = 0$ modes were found to be unstable (with no base flow or outer boundary). In panel (c), wherein only an axial field is applied, unstable disturbances are dampened similar to what was observed for $\chi_1 > \chi_2$.

Next, we apply azimuthal and axial fields simultaneously, generating a helical magnetic field. Figure 5 shows the effect of the helical field for the same parameter set as in Figure 2. If $\chi_1 > \chi_2$ region 1 can be stabilised and region 2 is shifted to the right (see panel (a)). As G increases, modes with $m < 0$ are rendered unstable first. Increasing the strength of the axial field dampens these modes, and we expect modes for which $mI + kZ = 0$ to be the most unstable (if they were unstable when $B = 0$). Comparing panel (b) to panel (a), where the strength of the axial field has doubled, larger $|m|, m < 0$ are now the first to go unstable as G increases. Irrespective of this, if the inner fluid is the more magnetic, increasing the magnetic field shifts region 2 further to the right. When $\chi_2 > \chi_1$, region 1 cannot be stabilised, and panels (c)-(d) show that modes $m \leq 0$ are rendered unstable when both field orientations are applied. Since region 2 comprises unstable short waves, these modes are stabilised by a strong enough axial field once $mI + Zk \neq 0$, irrespective of whether $\chi_1 < \chi_2$ or $\chi_1 > \chi_2$. Increasing J from $J = 1$ to $J = 100$ in panels (e) and (f) stabilises region 2 for the range of G considered ($G \leq 2.5 \times 10^4$) both when $B = 0$ and $B \neq 0$, but the range of unstable base flow strengths is larger than when $J = 1$.

We now focus on cases for which region 3 occurs. When there is no field, increasing J

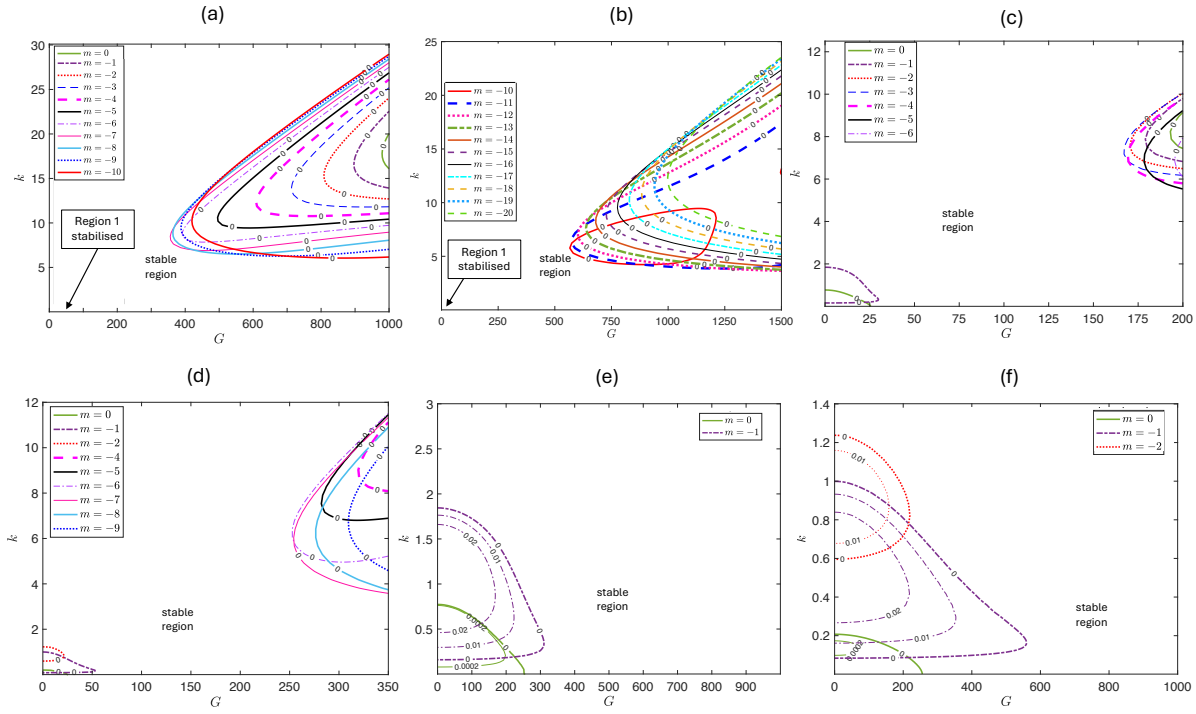

FIG. 5: Growth rates when $\mu = 0.5$, $R_2 = 1.3$, $R_0 = 0.1$, $W = 0$, $I = 1$, where $J = 1$ in (a)-(d), and $J = 100$ in (e)-(f). In (a)-(b) $B = 10$, $\chi_1 = 5$, $\chi_2 = 0$, with (a) $Z = 1$, (b) $Z = 2$. In (c)-(d) $B = 1$, $\chi_1 = 0$, $\chi_2 = 5$, with (c) $Z = 1$, (d) $Z = 2$. In (e)-(f) $B = 1$, $\chi_1 = 0$, $\chi_2 = 5$, with (e) $Z = 1$, (f) $Z = 2$. $m < 0$ modes can be the most unstable. If $\chi_1 > \chi_2$, region 1 is stabilised, and region 2 is pushed to the right as B or Z increases. If $\chi_2 > \chi_1$ increasing Z increases G_L, but region 2 is shifted further to the right, increasing G_R.

caused region 2 to shift to the right, so that when $J = 100$ region 2 no longer exists for $G \leq 2.5 \times 10^4$ in Figure 2(c), and a stable band of G exists between regions 1 and 3. In contrast, region 3 was practically unchanged upon increasing capillary forcing, since the unstable modes were found to be concentrated in critical layers at some distance from the fluid interface where surface tension acts (FBBM). It may be expected that since the field also interacts with the fluid solely through an interfacial condition, that it may also have little effect on these modes. Indeed, for low field strengths, region 3 unstable modes remain almost unchanged, whereas regions 1 and 2 are readily affected. However, we observe that a large enough B can influence the region 3 modes. Region 3 type modes are destabilised by an azimuthal field when $\chi_1 > \chi_2$, and by an axial field irrespective of which fluid is more magnetic. However, if $\chi_2 > \chi_1$, region 3 modes can be stabilised by a strong enough

azimuthal magnetic field. This is observed in Figure 6 when an azimuthal field is applied to the parameters of 2(c), where $B = 0$ and region 3 modes exist for $G \geq 1.508 \times 10^4$. When $\chi_1 > \chi_2$ in Figures 6(a) ($B = 100$) and 6(b) ($B = 500$), region 3 modes are destabilised at a lower G (at least $G < 1.4 \times 10^4$). By contrast, when $\chi_2 > \chi_1$ in Figure 6(c) ($B = 100$) region 3 modes are stabilised, shifting region 3 to $G > 1.519 \times 10^4$. Additionally, at these field strengths, new regions of instability may occur, which we name *magnetic regions*. In Figure 6(a) $B = 100$, region 3 persists and $m = 3, 4$ modes are rendered unstable, whilst $m = 2$ remains stable for the depicted window. An eigenfunction for an unstable mode in the $m = 3$ region is given in Figure 7(a) and shows the activity is located predominantly in the thicker fluid, and localised away from the boundaries. Increasing B further to $B = 500$ in Figure 6(b) renders $m \geq 0$ unstable, where two islands of unstable regions appear for $m = 0$, 1, 2. Eigenvalues associated with the upper region (see Figure 7(b) for an example) seem to belong to the magnetic region, with behaviour similar to the eigenfunction in Figure 6(a). On the other hand, the associated eigenfunctions for the lower sickle shaped regions (see Figure 7(c)) suggest a shear/region 3 mode has been excited by the magnetic field, since they display similar behaviour to eigenfunctions in region 3 (see Figure 7(d)). In Figure 6(c), the outer fluid is more magnetic, and region 3 retreats to the right at the field strength $B = 100$. But, increasing the field strength also renders smaller G unstable, and the band of stable G decreases with B.

A similar phenomenon occurs with an axial field alone, as can be seen in Figure 8. Region 3 extends to the left as the field strength is increased, and pockets of unstable magnetic regions appear when $B = 100$ (see panel (a)), at lower G than for the azimuthal case, where two regions exist. The upper region consists of unstable modes with eigenfunctions typical of a magnetic region (see panel (b)) and the lower region seems to consist of excited shear (region 3-type) modes (see panels (c) and (d)). For the latter, the activity is located towards the boundaries, with some activity near the interface. Moreover, once B is large enough, the sickle shaped region grows, as more excited shear (region 3-type) modes are rendered unstable (see panel (e) where $B = 500$). Eventually, the sickle shaped region joins with region 3 as B increases. We observe this result when the outer fluid is more magnetic when $B = 500$ in panel (f).

The result of applying both field orientations simultaneously when $B = 100$ is shown in Figure 9. Panel (a) shows that when $Z = 1$ a larger range of G is unstable than when the

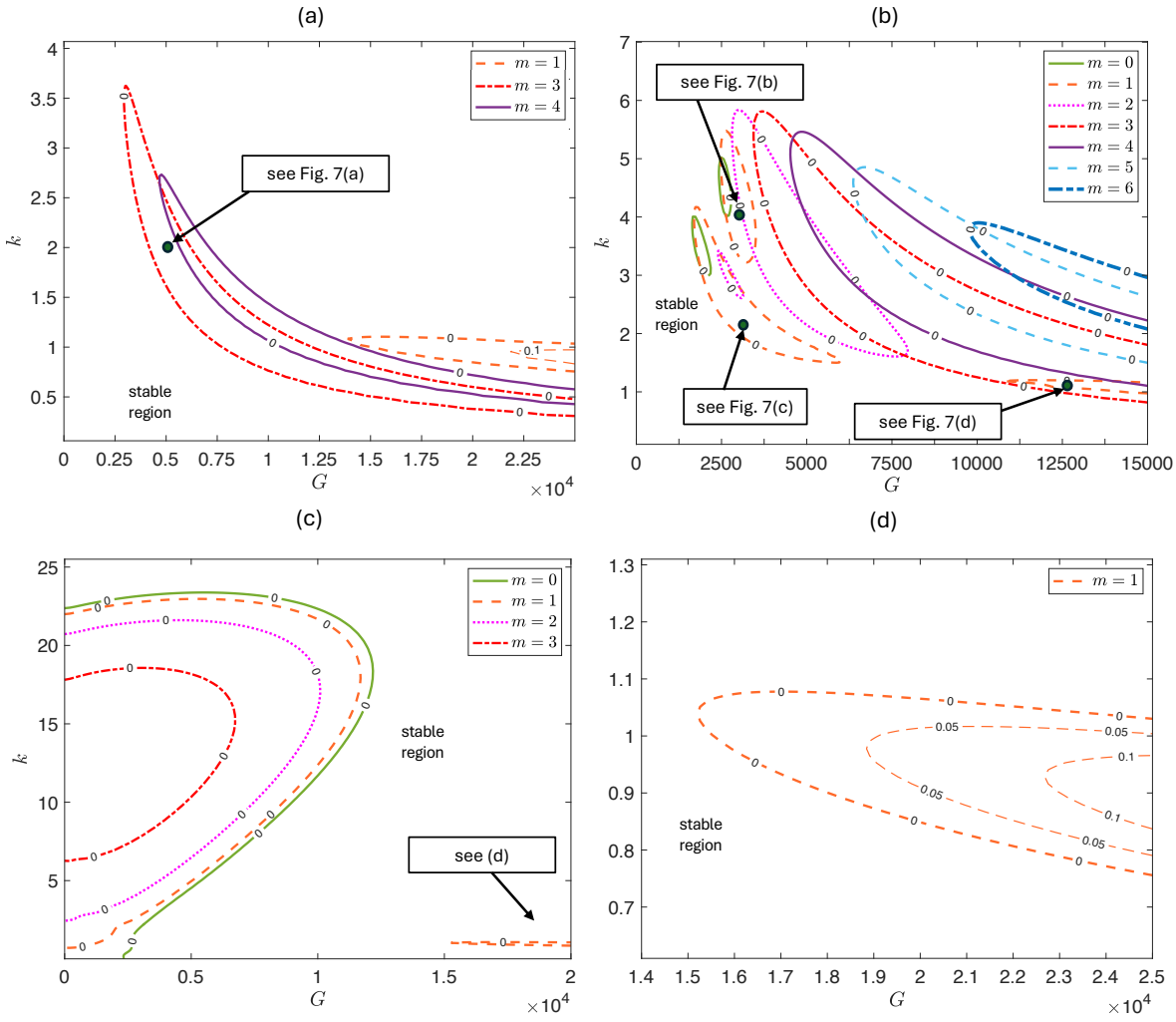

FIG. 6: Neutral curves for $m \geq 0$, when $\mu = 0.5$, $R_2 = 1.3$, $R_0 = 0.1$, $J = 100$, $W = 0$, $I = 1$, $Z = 0$. In (a) $B = 100$, $\chi_1 = 5$, $\chi_2 = 0$, (b) $B = 500$, $\chi_1 = 5$, $\chi_2 = 0$ and in (c) $B = 100$, $\chi_1 = 0$, $\chi_2 = 5$. (d) Region 3 enlarged. As B increases, it extends to the left when $\chi_1 > \chi_2$, but modes are stabilised when $\chi_2 > \chi_1$.

fields are applied independently. However, increasing the axial field strength from $Z = 1$ in panel (a) to $Z = 5$ in panel (b), shifts the magnetic region to the right, and produces a band of stable G extending from $G = 0$, where the critical G for instability is larger than for an independent axial or azimuthal field. In contrast, when $\chi_1 = 0$ and $\chi_2 = 5$ so that the outer fluid is more magnetic, we observe that both $Z = 1$ or $Z = 5$ are unstable for all G. The corresponding figure is not shown here for brevity. This phenomenon highlights the complexity of the problem, and shows that flow can drastically alter the magnetic effects. In particular, for no flow $\chi_1 > \chi_2$ is always stabilising with an azimuthal field, and here we

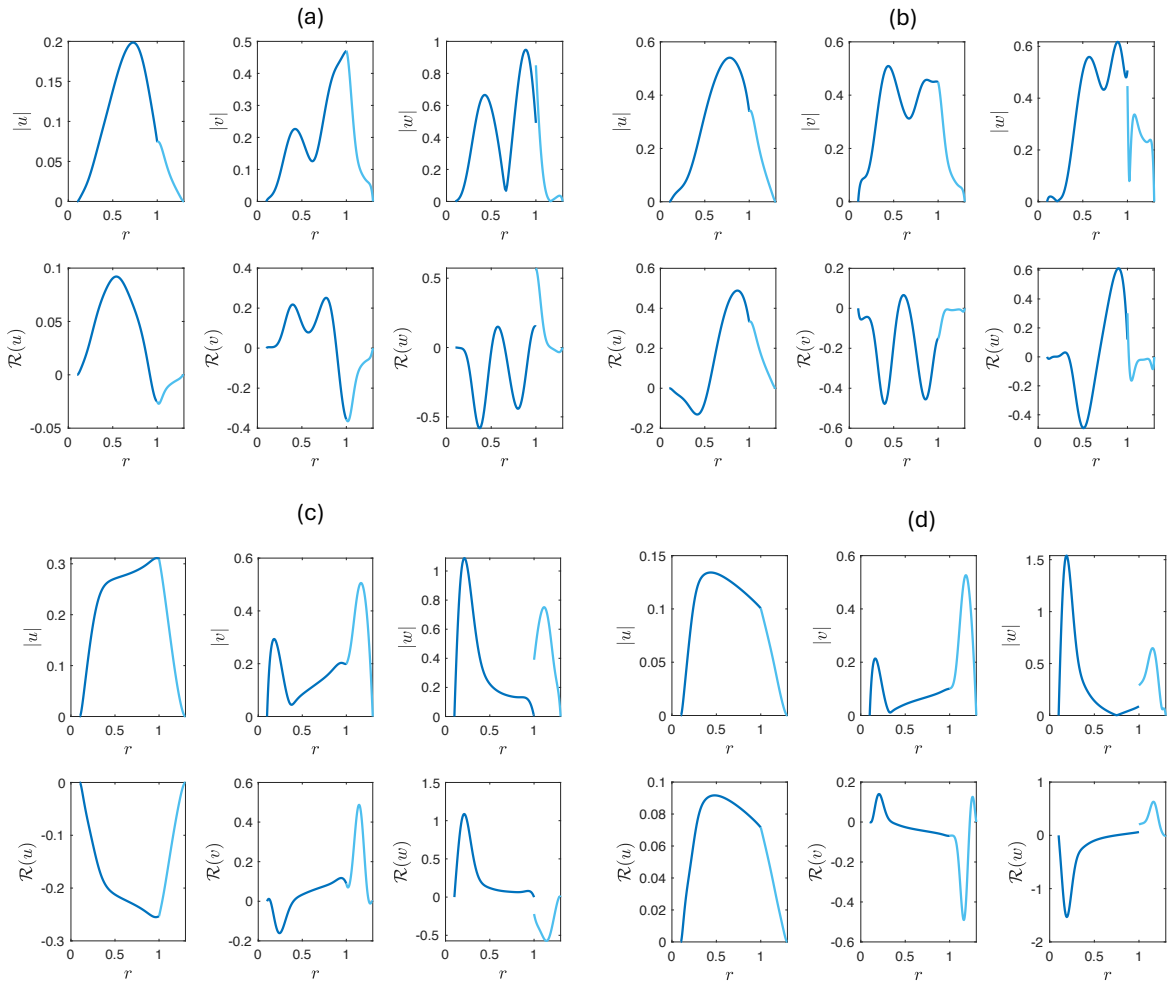

FIG. 7: Eigenfunctions when $\mu = 0.5$, $R_2 = 1.3$, $R_0 = 0.1$, $J = 100$, $W = 0$, $\chi_1 = 5$, $\chi_2 = 0$, $I = 1$, $Z = 0$. In (a) $B = 100$, $m = 3$, $k = 2$, $G = 5000$ when $s = 0.06088 - 25.88$i. In (b)-(d) $B = 300$, $m = 1$, where in (b) $k = 4$, $G = 3000$, $s = 0.042 - 31.695i$, (c) $k = 2$, $G = 3000$, $s = 0.036 - 7.958$i, (d) $k = 1.1$, $G = 12500$, $s = 0.011 - 14.223$i.

see a counter-example of this once $G \neq 0$. Figure 10 shows that when $G = 2 \times 10^4$, $B = 100$, then for given μ and R_2 a critical R_0 is needed for the magnetic region to occur. When $R_2 = 1.3$, $\mu = 0.5$ in (a), two regions of instability exist. The left hand region is typical of a magnetic region, and once the rod thickness exceeds a critical value it disappears, offering a stable flow for certain rod thicknesses at this field strength and pressure-gradient. Once the rod is too thick, or the inner fluid too thin, a hydrodynamical instability occurs. This is seen when $B = 0$ and it is dampened as the azimuthal field strength increases. We do not always find the magnetic region when region 3 exists. For example, region 3 occurs when

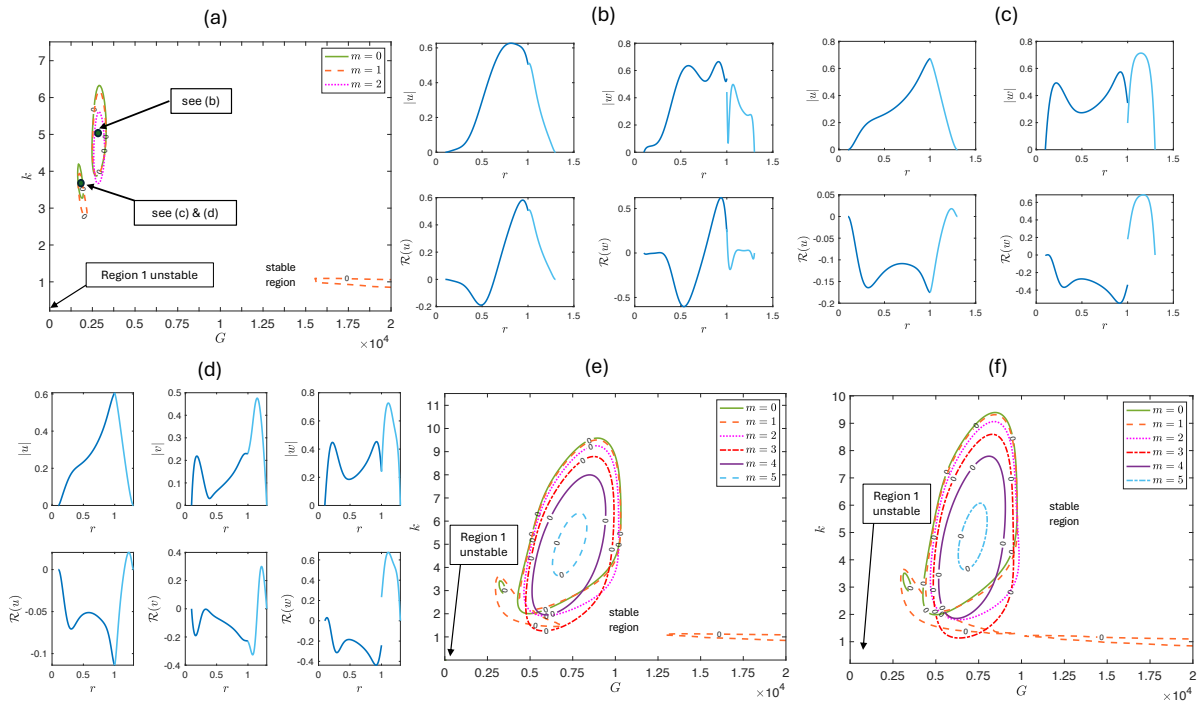

FIG. 8: Neutral curves for $m \geq 0$, when $\mu = 0.5$, $R_2 = 1.3$, $R_0 = 0.1$, $J = 100$, $W = 0$, $I = 0$. In (a) $BZ^2 = 100$, $\chi_1 = 5$, $\chi_2 = 0$, and eigenfunctions are given in (b) $m = 0$, $k = 0.5$, $G = 0.25 \times 10^4$, $s = 0.0012 - 33.75\text{i}$, (c) $m = 0$, $k = 3.5$, $G = 0.18 \times 10^4$, $s = 0.0088 - 8.25\text{i}$, and (d) $m = 1$, $k = 3.5$, $G = 0.18 \times 10^4$, $s = 0.0012 - 8.24\text{i}$. In (e) $BZ^2 = 500$, $\chi_1 = 5$, $\chi_2 = 0$. In (f) $BZ^2 = 500$, $\chi_1 = 0$, $\chi_2 = 5$. Region 3 grows to the left, irrespective of which fluid is magnetic. The sickle shaped region has eigenfunctions similar to region 3- type modes, with heightened activity at the interface. Two distinct regions of $m = 1$ region 3 - type modes exist in (a) and (c), and they have joined in (d). The upper regions consist of modes with eigenfunctions displaying the behaviour of *magnetic-region modes.*

$\mu = 1.5$, $R_2 = 2.0$, $R_0 = 0.45$, $J = 100$, and $5.65 \times 10^4 \leq G$, but the magnetic region does not occur for $0 < B < 1000$ at least and $G \leq 6.5 \times 10^4$. We do however see the region for different R_2, R_0 values with $\mu > 1$. This is shown in Figure 10(b) when $R_2 = 2.0$, $\mu = 1.5$. Here, a sufficiently thick rod is first necessary for stability, and then a thicker rod (or a thinner inner fluid) is then needed for the magnetic region to occur. We surmise that it is the thickness of the fluid layers and a large enough field strength that is essential for the magnetic region to exist. We observe that the behaviour of regions 1, 2, and 3 for other values of μ is analogous to that described when $\mu = 0.5$, even when $\mu > 1$.

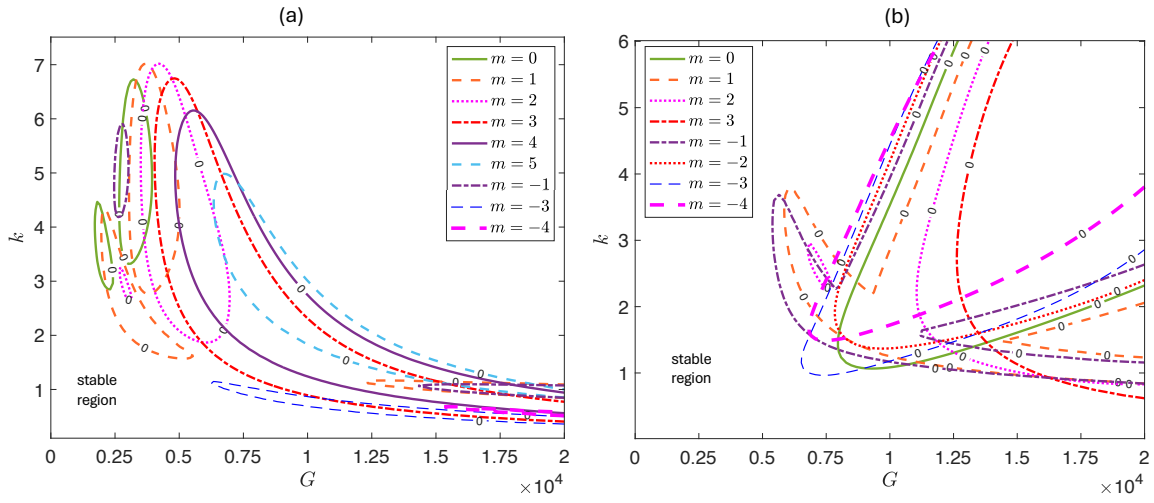

FIG. 9: Neutral curves when $\mu = 0.5$, $R_2 = 1.3$, $R_0 = 0.1$, $J = 100$, $W = 0$, $B = 100$, $\chi_1 = 5$, $\chi_2 = 0$, $I = 1$. In (a) $Z = 1$, (b) $Z = 5$. Increasing the axial field strength, increases the range of stable G, pushing the magnetic region to the right.

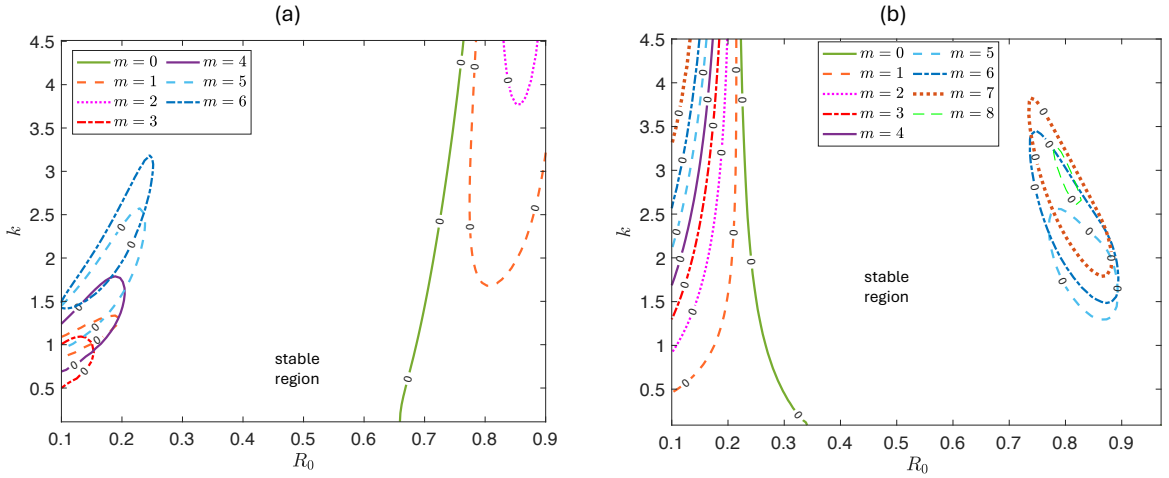

FIG. 10: Neutral curves for $m \geq 0$, when $G = 20000$, $J = 100$, $W = 0$, $B = 200$, $\chi_1 = 5$, $\chi_2 = 0$, $I = 1$, $Z = 0$. In (a) $\mu = 0.5$, $R_2 = 1.3$, and in (b) $\mu = 1.5$, $R_2 = 2.0$.

Certain configurations are unstable for all G with a stationary rod when $B = 0$. For example, if R_0 or R_2 is increased past a critical value, or, if R_0 is too small when $\mu > 1$, the system is unstable for all G ([31], FBBM). An azimuthal field when $\chi_1 > \chi_2$ will stabilise such systems as B is increased, and pushes the unstable region to the right. This is shown in Figure 11 for $R_0 = 0.9, R_2 = 1.3$ when $J = 1$ (panels (a) $B = 0$ and (b) $B = 100$) and $J = 100$ in (panels (c) $B = 0$ and (d) $B = 100$). Similarly, applying an azimuthal field allows

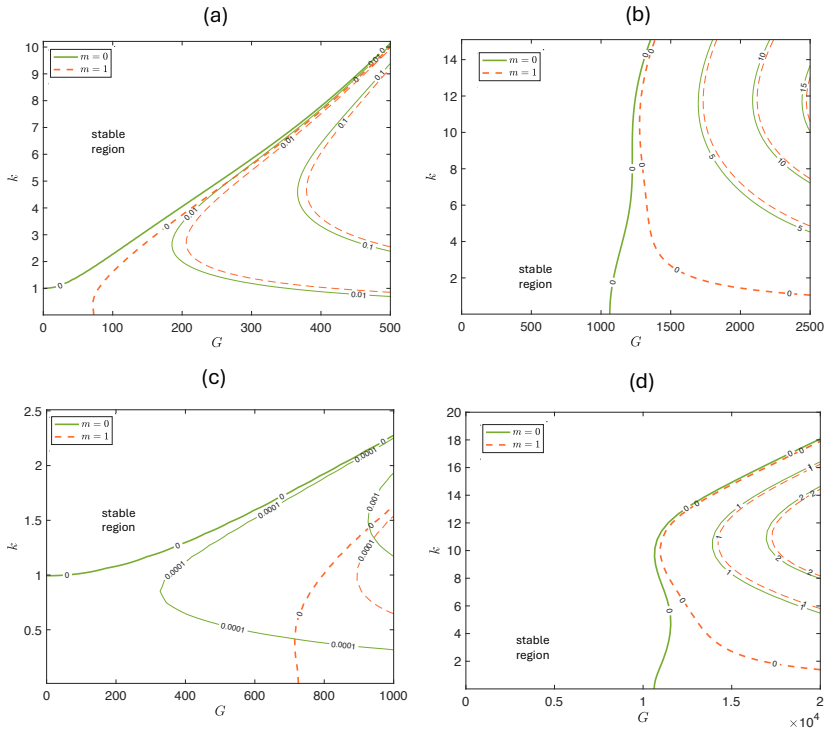

FIG. 11: Growth rates when $\mu = 0.5$, $R_2 = 1.3$, $R_0 = 0.9$, $\chi_1 = 5$, $\chi_2 = 0$, $I = 1$, $Z = 0$ for (a) $J = 1$, $B = 0$ (FBBM), (b) $J = 1$, $B = 100$, (c) $J = 100$, $B = 0$ (FBBM), (d) $J = 100$, $B = 100$. Increasing B shifts the unstable region to the right.

for a stable system with a thin rod and the outer fluid more viscous. Furthermore, $k = 0$ remains unstable for an axial field, as it did for region 1, and similarly adding an axial and azimuthal field simultaneously can only offer stability if $\chi_1 > \chi_2$. Figures for these results are omitted, as they display qualitatively similar patterns to those already presented.

A special case occurs when $\mu = 1.5$, $R_2 = 2.0$, $R_0 = 0.9$ in Figure 12, when for $B = 0$, there is instability for all G. The neutral curves when $J = 1, B = 0$ are given in Figures 12(a) and 12(b). In Figure 12(c), the effect of an azimuthal field is considered when the inner fluid is more magnetic ($\chi_1 = 5, \chi_2 = 0$), $B = 1$ and $J = 1$. Region 2 is pushed to the right slightly when $B = 1$, and region 1 is stabilised, but a region of $m = 1$ modes remain unstable, despite $m = 2$ unstable modes vanishing. Increasing B pushes $m = 1$ unstable modes in the lower region to the right, and region 2 is also pushed to higher G. When $J = 100$, region 2 does not exist when $B = 0$, and we find complete stability for $G \leq 2 \times 10^4$ when $B = 200$. The corresponding figure is omitted, as the behaviour is straightforward. But increasing B further causes the unstable magnetic region to appear, as shown in (c) when $B = 300$.

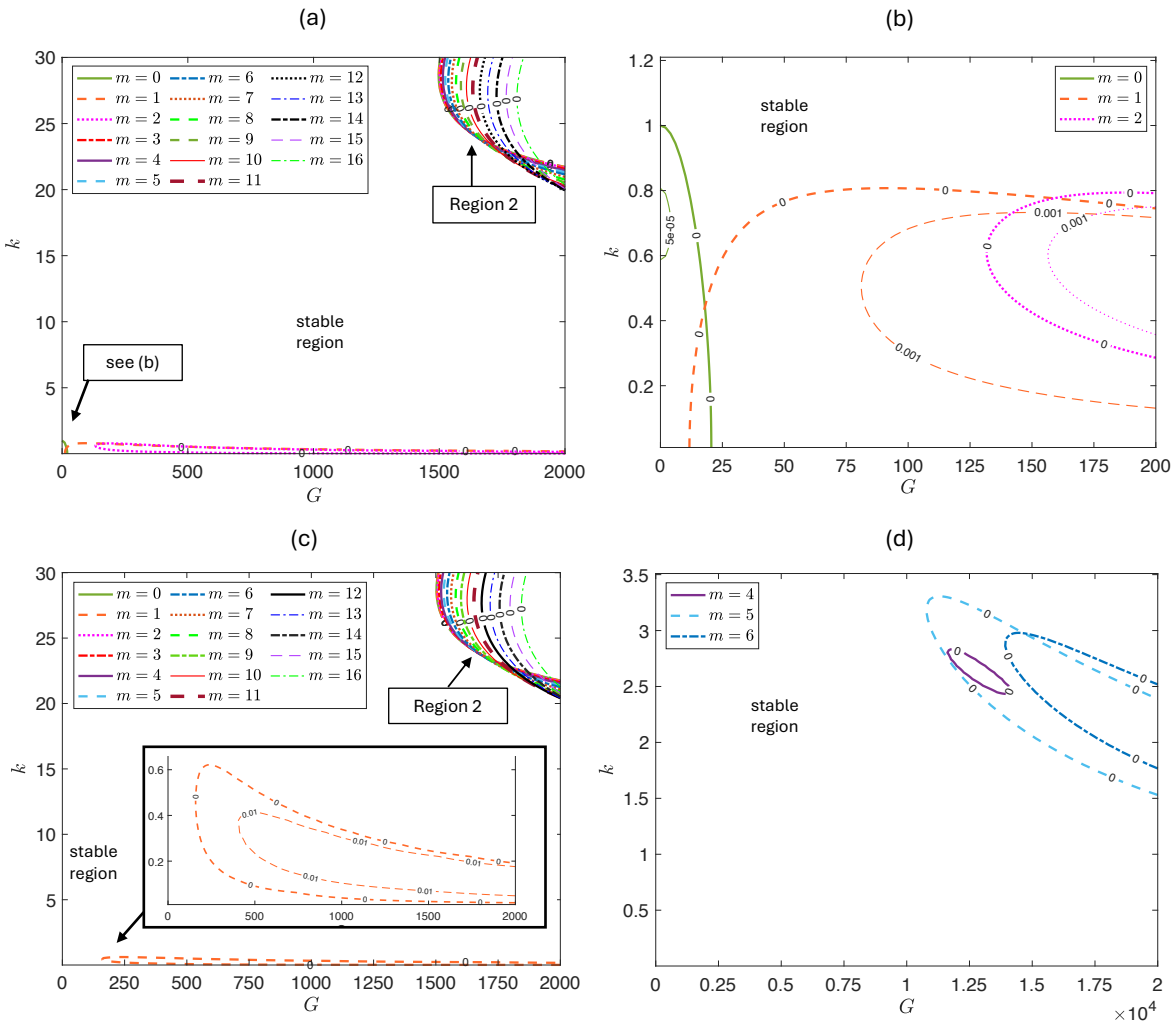

FIG. 12: Growth rates when $\mu = 1.5$, $R_2 = 2$, $R_0 = 0.9$, $W = 0$, $\chi_1 = 5$, $\chi_2 = 0$, $I = 1$, $Z = 0$, and in (a) $J = 1$, $B = 0$, where (b) shows an enlarged image of the lower region (FBBM), in (c) $J = 1$, $B = 1$, (d) $J = 100$, $B = 300$. An azimuthal field has a stabilising effect, but past a critical strength unstable magnetic modes appear.

In general, when the rod is stationary, a stable configuration can always be found for certain field strengths and orientations when $\chi_1 > \chi_2$. A caveat to this is when region 3 modes exist. The outer fluid can be more magnetic for $G \neq 0$, if long waves are stable when $B = 0$. Here, an axial field is necessary to produce a stabilising effect, with or without an azimuthal field. Should the field strength get too large, and one fluid be appropriately thinner than the other, magnetic unstable modes could occur.

B. Moving rod: $W \neq 0$

We now consider the case when the rod is moving either in the direction of the pressure-driven flow ($W > 0$) or in the opposite direction ($W < 0$). We determine the effect of adding azimuthal and/or axial fields. In Section III A it was observed that in general the effect of an azimuthal field is destabilising (except for region 3) if $\chi_2 > \chi_1$, but stabilising otherwise. In contrast, the effect of an independent axial field is the same whether $\chi_1 > \chi_2$ or $\chi_2 > \chi_1$. We focus on the case when the inner fluid is the more magnetic, and set $\chi_1 = 5$ and $\chi_2 = 0$.

If regions 1, 2 and 3 exist when there is no field and $W = 0$, translating the rod can shift the regions to produce different ranges of stable G (FBBM). In these cases, the effect of an axial and/or azimuthal field on the shifted regions is qualitatively similar to what was found in Section III A for $W = 0$, and so it is not discussed further here. Often by translating the rod, modes are rendered unstable, and for rod speeds that shift region 3 to the right, small G becomes unstable when $B = 0$ as indicated by the roots of the small k formula (51). This is shown by comparing Figure 2(c) where $W = 0$, with Figures 13(a) and 13(b), where $W = 1000$ and $W = -1000$, respectively. Figure 13(c) shows that an azimuthal magnetic field dampens the left-hand unstable region in Figure 13(a), to achieve complete stabilisation for $G < G_c$ when $B = 100$, where for $G \geq G_c$ the magnetic region and region 3 both exist. Upon comparing Figure 6(a) where $W = 0$, with Figure 13(c) where $W = -1000$, we observe that the regions of instability are modified by translating the rod, and the magnetic region requires a stronger G when $W = -1000$ than when the rod is stationary. In contrast, we find that $W > 0$ results in the magnetic region spanning a larger range of G, as well as requiring a lower critical field strength to appear. For example, when $W = 1000$ in panel (d), a magnetic region appears for a larger range of G when $B = 40$, than in panel (c) where $B = 100$.

In the non-magnetic case, translating the rod can produce a window of stable G, that does not exist when $W = 0$. This window is bounded by a left-most unstable region and a right-most unstable region. Figure 14(a) shows an example of this when $B = 0$ and the rod speed is such that $W = 50$. We observe that, when $\chi_1 > \chi_2$, increasing the azimuthal magnetic field strength will decrease the area of the left-hand unstable region so that it disappears completely for strong enough B, and shifts the right-hand region to the right. This is shown in panel (b) of Figure 14 when B is increased from $B = 0$ in panel (a) to $B = 10$. Although an axial field alone cannot stabilise long-waves, it can be applied in conjunction

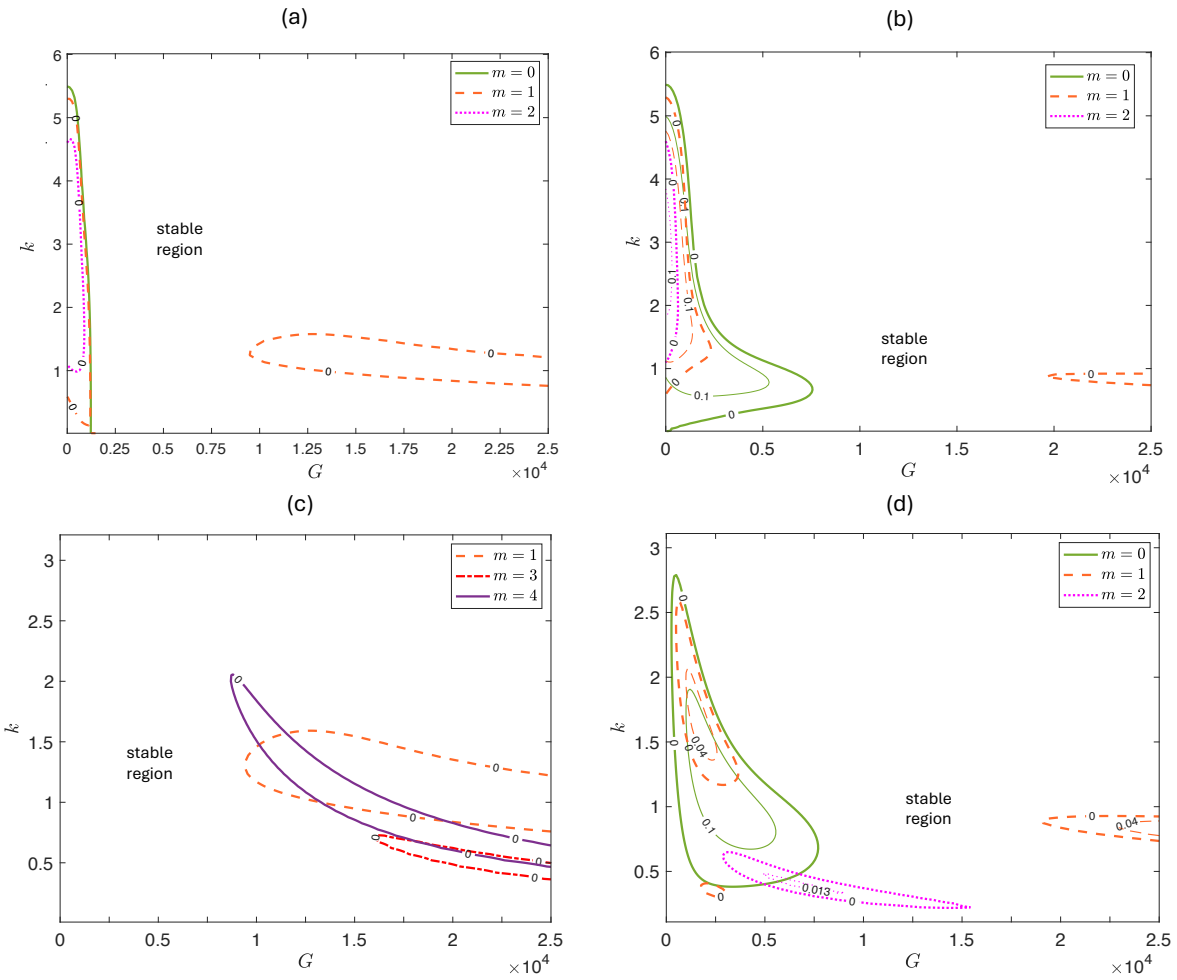

FIG. 13: Growth rates when $\mu = 0.5$, $R_2 = 1.3$, $R_0 = 0.1$, $\chi_1 = 5$, $\chi_2 = 0$, $I = 1$, $Z = 0$, and in (a) $W = -1000$, $B = 0$ (FBBM), (b) $W = 1000$, $B = 0$ (FBBM), (c) $W = -1000$, $B = 100$, (d) $W = 1000$, $B = 40$. An azimuthal field stabilises instabilities caused by the moving rod at low G, but unstable magnetic modes can be triggered.

with the azimuthal field to produce stabilising effects. Nevertheless, $m < 0$ become the most dangerous in a similar fashion to Section III A, and can be unstable for a given G when $m > 0$ is stable. This is shown in panel (c) where an axial and azimuthal field are applied with $B = 10$, $Z = 5$. Increasing B to $B = 100$ in panel (d) stabilises the $m < 0$ modes for this range of G, and only the right hand region of $m = 0$ unstable modes remain. Increasing B further shifts this unstable region to the right, increasing the range of stable G. For other parameter values where such a window exists, bounded unstable regions like in Figure 14(a), we observe the field having a similar effect.

In Figure 15(a), where $W = 100$, (c.f. Figure 12a for $W = 0$) the window of stable G is bounded differently from Figure 14(a). Here, region 2 in panel 15(a) behaves as expected, and the lower unstable region is stabilised with an azimuthal field. However, in the presence of a helical field and a moving rod, the lower region behaves somewhat unexpectedly. This is shown in Figure 15(b), where the growth rates are plotted for small k (region 2 exists at larger k). Here, an azimuthal and axial field are applied in tandem, stabilising all $m = 1$, 2 modes, and reducing the area of the unstable $m = 0$ region, whilst a pocket of unstable $m = -1$ modes remains, located above the $m = 0$ region. We observe that increasing Z causes these two regions to expand, increasing the range of unstable G. Yet, they disappear by increasing B and retaining $Z = 1$. Additionally, panel (c) shows that in the non-magnetic case, a region of instability can exist at moderate wave number when the rod speed is too large ($W = 500$ in panel (c)). We observe stabilisation of this region for either an azimuthal field (if $\chi_1 > \chi_2$) or an axial field, since $k > 0$ is unstable when $B = 0$.

Often for no pressure gradient ($G = 0$), a range of rod speeds could produce stability (FBBM). In these examples, a window of stable W exists, bounded by a left-hand and right-hand unstable region, resembling Figure 14(a). We observe that in the presence of the magnetic field the regions behave similarly to what was observed in Figure 14. However, for some configurations the system is unstable for all $W \geq 0$ when $G = 0$. We find an azimuthal field can produce a range of stable rod speeds if the inner fluid is more magnetic. An example is given in Figure 16. In panel (a) the system is unstable for all W when $B = 0$, but increasing B to $B = 100$ in panel (b) produces a range of stable $W \geq 0$. This occurs analogously to configurations that were unstable for all G when $W = 0$ in Figure 11. We observe similar effects for unstable configurations when both W and G are non-zero. Nevertheless, the magnetic region can still appear for certain ratios of thicknesses of the fluids, and this occurs for the parameter set in Figure 16 once B is increased to $B = 200$ in panel (c).

Translating the rod adds another parameter to an already large parameter set, and we have therefore discussed only a small number of cases here. In general, we would expect an azimuthal field to have a stabilising effect if the inner fluid is more magnetic, so long as it is below the strength for the onset of magnetic instabilities. An axial field could stabilise a system so long as $k = 0$ is stable when $B = 0$. Applying both fields in tandem should be taken with caution when in conjunction with the moving rod, since it does not always

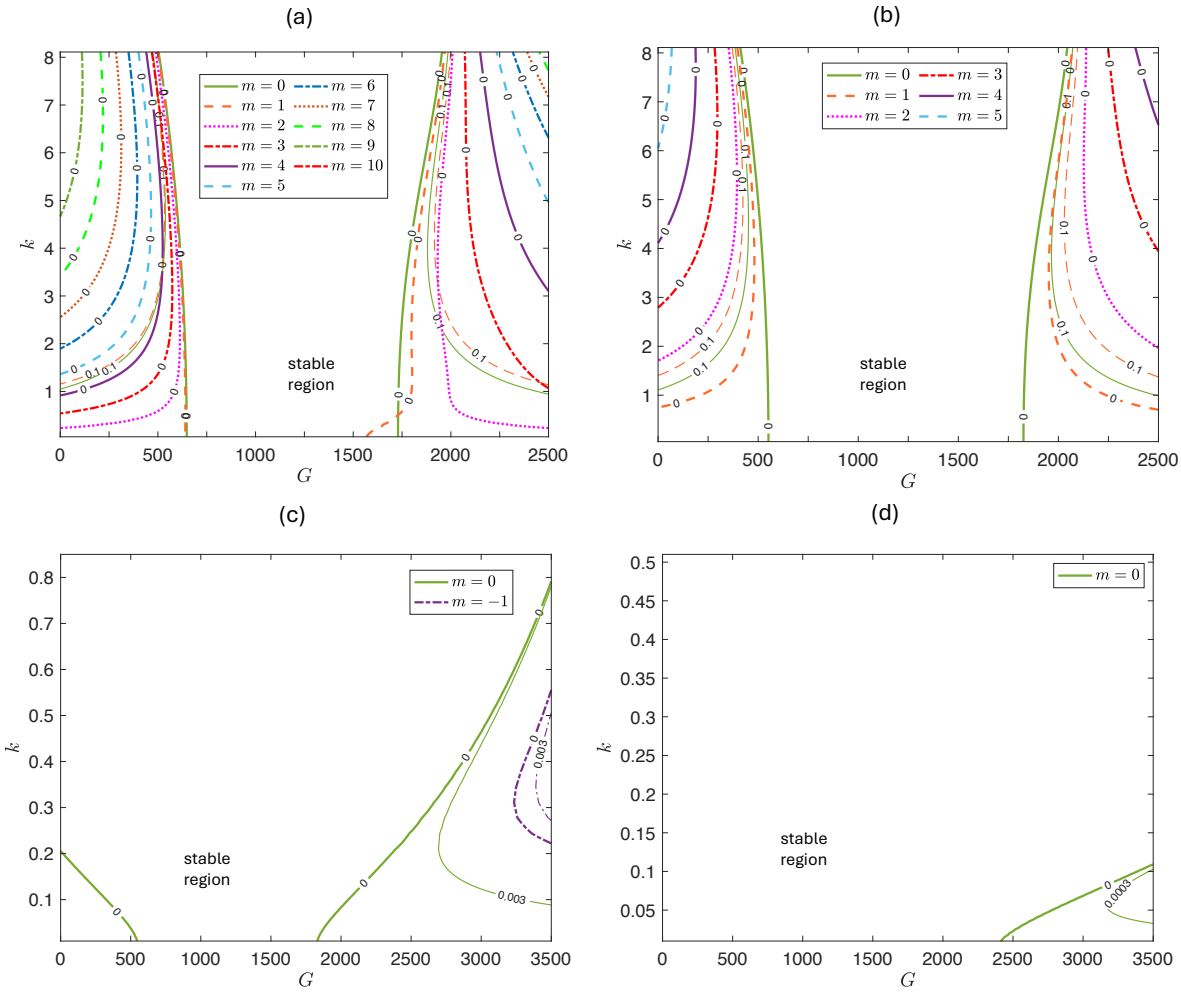

FIG. 14: Growth rates when $\mu = 0.5$, $R_2 = 1.3$, $R_0 = 0.9$, $J = 1$, $W = 50$, $\chi_1 = 5$, $\chi_2 = 0$, and in (a) $B = 0$ (FBBM) (b) $B = 10$, $I = 1$, $Z = 0$, (c) $B = 10$, $I = 1$, $Z = 5$, (d) $B = 100$, $I = 1$, $Z = 5$.

behave in a clear trend, or by the manner described in Section III A, and Figure 15 gives an example of this.

IV. CONCLUDING REMARKS

We have studied the effect of a magnetic field on a rod-annular flow (RAF). The rod is either stationary or translates along its axis at a prescribed speed. Although the results that we have presented apply for a small set of the possible parameter values, we have nevertheless observed some general trends. A weak axial field always has a stabilising influence irrespec-

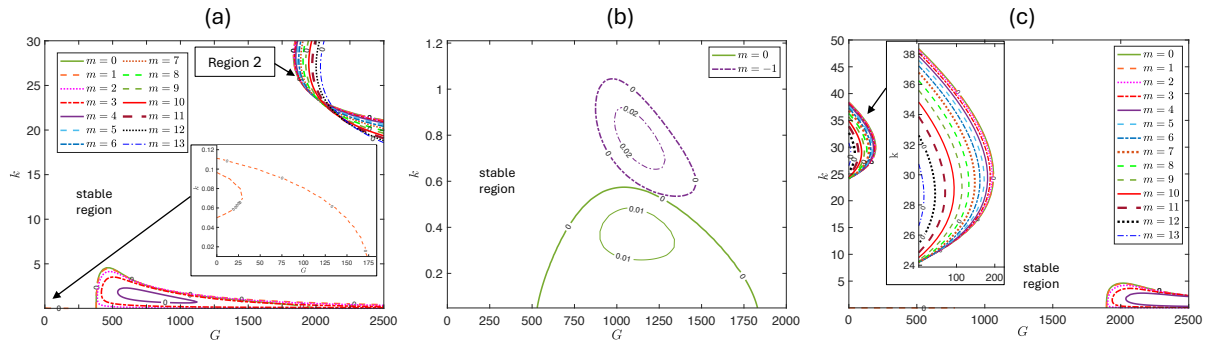

FIG. 15: Growth rates when $\mu = 1.5$, $R_2 = 2$, $R_0 = 0.9$, $J = 1$, $\chi_1 = 5$, $\chi_2 = 0$, where in (a) $W = 100$, $B = 0$ and in (b) $W = 100$, $B = 100$, $I = 1$, $Z = 1$. In (c) $W = 500$, $B = 0$. Panels (a) and (c) are adapted from FBBM.

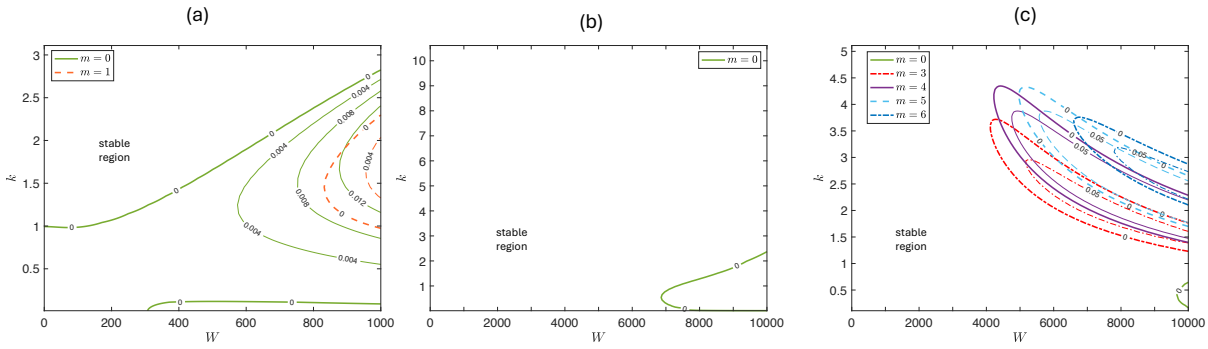

FIG. 16: Growth rates when $G = 0, \mu = 0.5$, $R_2 = 1.3$, $R_0 = 0.1$, $J = 100$, $\chi_1 = 5$, $\chi_2 = 0$, $I = 1$, $Z = 0$ and in (a) $B = 0$, (b) $B = 100$, (c) $B = 200$.

tive of which fluid has the higher magnetic susceptibility. In contrast a weak azimuthal field will only be stabilising if the inner fluid is the more magnetic. The latter agrees with the ferrohydrodynamic literature when there is no base flow [15–17, 19, 20, 22]. An axial field cannot stabilise long waves, and therefore an azimuthal field is required if hydrodynamically unstable long waves are to be suppressed. Adding an azimuthal field alongside an axial field can dampen these modes, provided the inner fluid is the more magnetic. Applying an azimuthal and axial field simultaneously gives rise to a helical field and in this case often the least stable modes are those parallel to the field on the interface, so that $\overline{\boldsymbol{H}} \cdot \nabla\zeta = 0$ or $mI + kZ = 0$, requiring $m < 0$. These are akin to the troublesome 'tearing modes' in Tokamak design [36]. If $\chi_1 > \chi_2$ the azimuthal field may control these modes, but if $\chi_1 < \chi_2$ hydrodynamic effects will be required and the field cannot then be too strong.

In general instabilities that occur at large base flow strengths require stronger field strengths to be suppressed (in particular region 2). Region 3 modes are largely unaffected by weak fields, and for strong fields they don't behave as we might expect; the growth rate is increased by an azimuthal field when the inner fluid is more magnetic. Moreover, a strong enough magnetic field can destabilise region 3 modes, with an azimuthal field (if the inner-fluid is more magnetic) and an axial field. Since region 3 modes are hardly influenced by interfacial effects, this suggests that the field may be having a non-local effect, despite it only coupling with the flow through the normal-stress condition at the interface. Indeed, the field varies spatially, and experiences discontinuities at the rod, interface and wall. Strong fields can also induce new magnetic instabilities for both independent and combined field orientations. These exist for a range of base flow strengths that depend on the parameters of the system. These seem to occur at critical thicknesses of the two fluids, and don't necessarily occur if region 3 modes are present. Indeed, it seems unlikely that it is the presence of the boundaries that cause these modes, due to the heightened activity in the eigenfunctions near both the interface and within the thicker fluid (e.g. Figures 7(a),(b) and 8(a),(b)).

Crucially, an axial rod is required to generate the azimuthal field needed to dampen unstable long waves that occur at low base flow strengths. Nevertheless, our results suggest that regular core-annular flow (CAF), for which the rod is absent, could be stable in the presence of an axial field if the base flow is strong enough to control the capillary-driven instabilities ($m = 0$, $k < 1$).

We have provided representative cases of all the observed behaviour. However, given the vast parameter space for the problem, the question arises whether interesting regimes could be missed by too coarse a grid search. We are confident that we have identified all unstable regions in the figures we have presented. Sometimes small isolated islands of instability do appear, but warning of such behaviour is usually provided by the topology of the negative growth rate contours, which we omit for clarity. The problem is most sensitive to variations in the annular thicknesses, $1 - R_0$ and $R_2 - 1$ and some effects only appear for fairly thin layers. In contrast, the physical effects of varying the other parameters are more transparent and the overall picture tends not to change beyond a threshold.

The findings presented here are most relevant to ink-jet printing and magnetic drug targeting, and extend the work of the current ferrofluid literature by allowing for a two-fluid flow. They are also relevant to enhanced fluid transportation [7] and drag reduction

technologies [8], where ferrofluids are already used for lubrication.

To the best of our knowledge, no experiments have yet addressed the configuration studied here. Nonetheless, related experimental work [18], [37], demonstrates the feasibility of realising comparable systems such as ours. Finally, while we have restricted our attention to the linear regime, it should be remembered that in real flows it is possible that instabilities may saturate to form surface waves of significant amplitude. Moreover, some linearly stable configurations may be destabilised by sufficiently large amplitude disturbances. Future work could involve weakly nonlinear analysis to identify subcritical bifurcations, while a non-modal approach [38] could highlight transient growth mechanisms.

---

[1] C. Scherer and A. M. Figueiredo Neto, Ferrofluids: Properties and applications, Brazil. J. of Phys. **35**, 718 (2005).

[2] S. W. Charles, Some applications of magnetic fluids— use as an ink and in microwave systems, J. Magnet. Mag. Mater. **65**, 350 (1987).

[3] A. R. Abdel F., S. Ghosh, and I. K. Puri, Printing microstructures in a polymer matrix using a ferrofluid droplet, J. Magnet. Mag. Mater. **401**, 1054 (2016).

[4] P. A. Voltairas, D. I. Fotiadis, and L. K. Michalis, Hydrodynamics of magnetic drug targeting, J. Biomech. **35**, 813 (2002).

[5] M. Asfer, S. K. Saroj, and P. K. Panigrahi, Retention of ferrofluid aggregates at the target site during magnetic drug targeting, J. Magnet. Mag. Mater. **436**, 47 (2017).

[6] V. C. Gonella, F. Hanser, J. Vorwerk, S. Odenbach, and D. Baumgarten, Influence of local particle concentration gradient forces on the flow-mediated mass transport in a numerical model of magnetic drug targeting, J. Mag. Magnet. Mater. **525**, 167490 (2021).

[7] M. D. Contreras-Mateus, A. Chaves-Guerrero, F. H. Sánchez, and N. N. Nassar, Ferrofluids and magnetism in the oil industry: Theories, challenges, and current applications—A comprehensive review, Phys. Fluids **36**, 121302 (2024).

[8] M. M. Neamtu-Halic, M. Holzner, and L. M. Stancanelli, Drag reduction utilizing a wall-attached ferrofluid film in turbulent channel flow, J. Fluid Mech. **996**, A35 (2024).

[9] L. Preziosi and F. Rosso, Interfacial stability in a two-layer shearing flow between sliding pipes, Eur. J. Mech. B, Fluids **10**, 269 (1991).

[10] A. G. Walton, The linear and nonlinear stability of thread-annular flow, Phil. Trans. Roy. Soc. **363**, 1223 (2005).

[11] L. Rayleigh, On The Instability Of Jets, Proc. Lond. Math. Soc. **s1-10**, 4 (1878).

[12] S. Tomotika, On the instability of a cylindrical thread of a viscous liquid surrounded by another viscous fluid, Proc. Roy. Soc. Lond. A **150**, 322 (1935).

[13] R. M. Christiansen and A. N. Hixson, Breakup of a Liquid in a Denser Liquid, Ind. & Eng. Chem. **49**, 1017 (1957).

[14] B. J. Meister and G. F. Scheele, Drop formation from cylindrical jets in immiscible liquid systems, AIChE J. **15**, 700 (1969).

[15] V. G. Bashtovoi and M. S. Krakov, Stability of an axisymmetric jet of magnetizable fluid, J. Appl. Mech. Tech. Phys. **19**, 541 (1979).

[16] V. I. Arkhipenko, Y. D. Barkov, V. G. Bashtovoi, and M. S. Krakov, Investigation into the stability of a stationary cylindrical column of magnetizable liquid, Fluid Dyn. **15**, 477 (1981).

[17] D. Rannacher and A. Engel, Cylindrical Korteweg–de Vries solitons on a ferrofluid surface, New J. Phys. **8**, 108 (2006).

[18] E. Bourdin, J.-C. Bacri, and E. Falcon, Observation of Axisymmetric Solitary Waves on the Surface of a Ferrofluid, Phys. Rev. Lett. **104**, 094502 (2010).

[19] R. Canu and M.-C. Renoult, Linear stability analysis of a Newtonian ferrofluid cylinder under a magnetic field, J. Fluid Mech. **915**, A137 (2021).

[20] R. Canu and M.-C. Renoult, Linear stability analysis of a Newtonian ferrofluid cylinder surrounded by a Newtonian fluid, J. Fluid Mech. **927**, A36 (2021).

[21] V. M. Korovin, Capillary disintegration of a configuration formed by two viscous ferrofluids surrounding a current-carrying conductor and having a cylindrical interface, Tech. Phys. **49**, 669 (2004).

[22] S. H. Ferguson Briggs and A. J. Mestel, Linear stability of a ferrofluid centred around a current-carrying wire, J. Fluid Mech. **942**, A20 (2022).

[23] M. G. Blyth and E. I. Părău, Solitary waves on a ferrofluid jet, J. Fluid Mech. **750**, 401 (2014).

[24] A. Doak and J.-M. Vanden-Broeck, Travelling wave solutions on an axisymmetric ferrofluid jet, J. Fluid Mech. **865**, 414 (2019).

[25] P. J. Redberger and M. E. Charles, Axial laminar flow in a circular pipe containing a fixed eccentric core, Canad. J. Chem. Eng. **40**, 148 (1962).

[26] D. D. Joseph, K. Nguyen, and G. S. Beavers, Non-uniqueness and stability of the configuration of flow of immiscible fluids with different viscosities, J. Fluid Mech. **141**, 319 (1984).

[27] D. D. Joseph, M. Renardy, and Y. Renardy, Instability of the flow of two immiscible liquids with different viscosities in a pipe, J. Fluid Mech. **141**, 309 (1984).

[28] L. Preziosi, K. Chen, and D. D. Joseph, Lubricated pipelining: Stability of core-annular flow, J. Fluid Mech. **201**, 323 (1989).

[29] H. H. Hu and D. D. Joseph, Lubricated pipelining: Stability of core-annular flow. Part 2, J. Fluid Mech. **205**, 359 (1989).

[30] S. H. Ferguson Briggs, M. G. Blyth, and A. J. Mestel, Stability of a two-fluid rod annular flow, Phys. Rev. Fluids **10**, 034001 (2025).

[31] H. A. Dijkstra, The coupling of interfacial instabilities and the stabilization of two-layer annular flows, Phys. Fluids **4**, 1915 (1992).

[32] C. J. Heaton, Linear instability of annular Poiseuille flow, J. Fluid Mech. **610**, 391 (2008).

[33] M. Weinstein, The effect of a vertical magnetic field on the capillary instability of a liquid—liquid jet, J. Frank. Inst. **325**, 537 (1988).

[34] S. H. Ferguson Briggs, M. G. Blyth, and A. J. Mestel, The stability of two flowing coaxial ferrofluid annuli, Magnetohydrodnamics (2025).

[35] R. E. Rosensweig, *Ferrohydrodynamics* (Cambridge University Press, 1985).

[36] S. V. Mirnov and I. B. Semenov, Investigation of the instabilities of the plasma string in the Tokamak-3 system by means of a correlation method, Soviet Atomic Energy **30**, 22 (1971).

[37] R. Canu, A. Bouchet, and M.-C. Renoult, New experiments and theory on ferrofluid cylinder in an azimuthal magnetic field, Phys. Fluids **35**, 112116 (2023).

[38] R. R. Kerswell, Nonlinear Nonmodal Stability Theory, Annual Review of Fluid Mechanics **50**, 319 (2018).